APPENDIX B2 – DETAILED DESCRIPTION OF REEFMOD-GBR AND SIMULATION RESULTS

Yves-Marie Bozec and Peter J. Mumby

Marine Spatial Ecology Lab, School of Biological Sciences and ARC Centre of Excellence for Coral Reef Studies, University of Queensland, St Lucia, QLD 4072, Australia

With contributions from: Ken Anthony, Mark Baird, Line Bay, Scott Condie, Daniel Harrison, Karlo Hock, Robert Mason, Mikhail Matz, David Mead, Marji Puotinen, Cynthia Riginos, Cedric Robillot, Chris Roelfsema, Nicholas Wolff.

B2.1 General description

ReefMod is a spatially explicit model of coral population dynamics initially developed for Caribbean coral reefs (Mumby et al. 2007). The model has been continuously improved (Mumby et al. 2014, Bozec et al. 2015, 2016) and was recently adapted to simulate coral dynamics on a typical Pacific reef (Ortiz et al. 2014). The model is individual-based and simulates the settlement, growth and mortality of coral colonies with a six-month time step on a two-dimensional grid lattice of 20 × 20 cells each of which approximates 1m^2 of the reef floor (Fig. 27). Each grid cell can be occupied by multiple coral colonies of different functional groups and by a mixture of reef algae. The grid is toroidal (i.e. wrapped around) so that every cell has the same number of neighboring cells. While the spatial dynamics captured on a grid lattice are scale-invariant (i.e. larger domains give the same demographic outputs under the same environmental forcing), the variability of coral colonisation on a reef is reproduced through a stochastic initialisation of corals (randomised initial cover, size structure and placement on the grid) and the simulation of 40 replicate model runs for each parameter scenario.

Corals are modelled by their size and belong to six functional groups:

- Plating corals (e.g. *Acropora hyacinthus*, *Acropora cytherea*)
- Arborescent (staghorn) corals (e.g. *Acropora muricata*, *Acropora nobilis*, *Acropora robusta*)
- Corymbose/small branching acroporids (e.g. *Acropora millepora*, *Acropora humilis*)
- Pocilloporids and other non-acroporid corymbose (e.g. *Stylophora pistillata*)
- Small massive/submassive/encrusting corals (e.g. *Lobophylliidae*, favids, *Goniastrea*)
- Large massive (*Porites lutea*, *Porites lobata*, *Porites australiensis*).

A focus on Acropora corals is justified as they represent the key habitat-forming species on the Reef and account for around 70 percent of the coral biodiversity in the Indo-Pacific region (Wallace 1999). Other model agents include patches of long turf, encrusting fleshy (i.e. *Lobophora*) and upright fleshy macroalgae. Ecological interactions and coral demographics are explicit and occur at colony scales following probabilistic rules. Spatially explicit grazing maintains macroalgae in a cropped state, which facilitates coral settlement and growth. Acute disturbances such as bleaching, or cyclones can occur randomly or following specified scenarios. Their impact on corals is group-specific based on empirical observations.

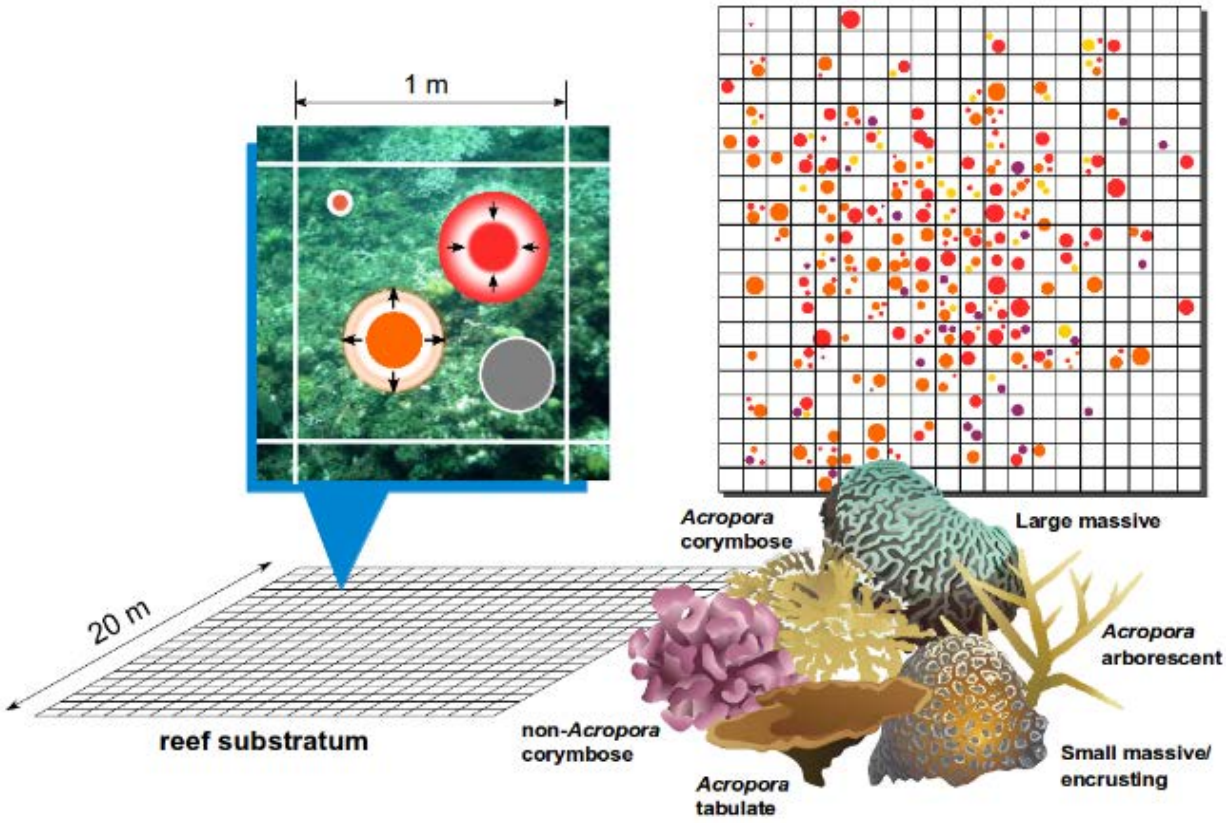

Figure 27: Schematic representation of the reef ecosystem model (ReefMod). Individual coral colonies are typified by circular areas of variable size. Corals settle, grow, shrink and die in a virtual 20m×20m environment as they do in situ. Demographic rates are specific to the six modelled coral groups. Graphics: IAN image library and YM Bozec.

For simulating coral dynamics on the Great Barrier Reef, ReefMod was further developed to integrate population dynamics of the coral-feeding crown-of-thorns starfish (*Acanthaster* spp). In addition, coral demographics were refined with explicit mechanisms driving the early-life stages of corals: coral reproduction, coral settlement, and growth and mortality of coral recruits and juveniles. A new parameterisation of coral recruitment, growth and mortality (including bleaching mortality) was developed based on recent empirical data from the Reef. For RRAP, we implemented natural processes of rubble formation and stabilisation which affect coral juvenile demographics. The model was also augmented with recent modelling of algal succession dynamics and grazing (Bozec et al. 2019); however, due to limited data on fish abundance and body size, we assumed full grazing efficiency across the entire Reef, so that reef algae were maintained in a cropped state everywhere. The process of grazing will be revisited in the RRAP R&D Program by modelling functional fish grazing for different levels of fishing and habitat complexity (Mumby 2006, Bozec et al 2013, 2016) and by accounting for spatial and temporal variations in algal productivity as informed by the eReefs biogeochemical model (Chen et al. 2011, Herzfeld et al. 2016). These new implementations lead to a comprehensive representation of key reef processes and interactions (Fig 28).

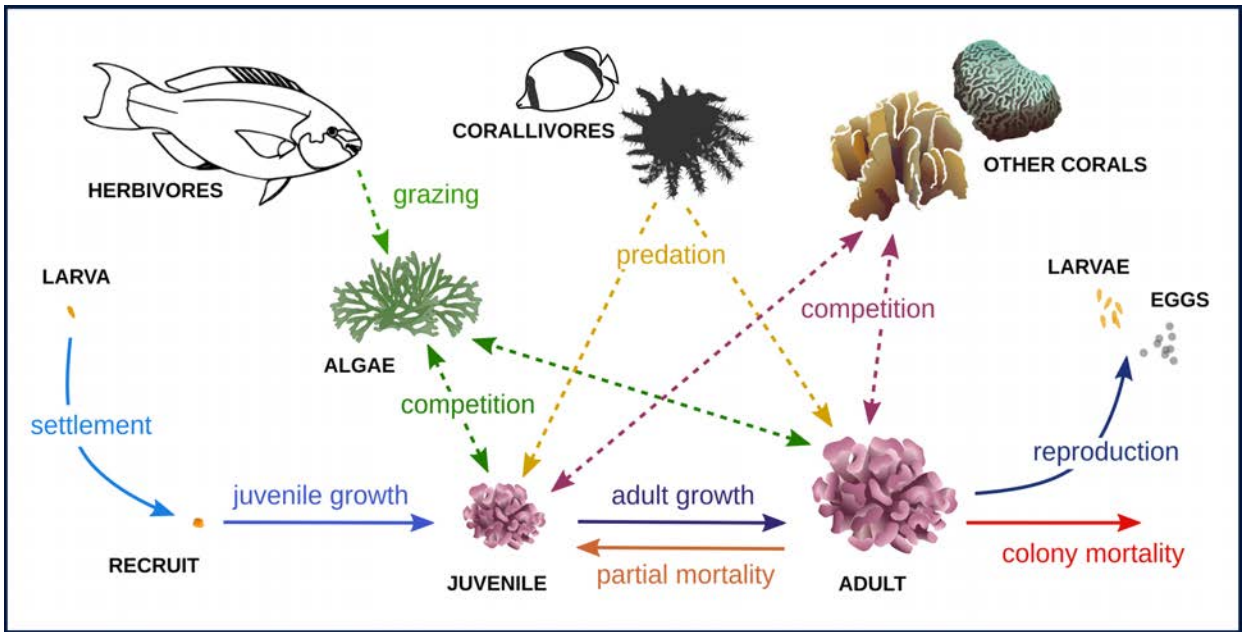

Figure 28: Demographic processes (solid arrows) and ecological interactions (dashed arrows) affecting corals in the reef ecosystem model (ReefMod). Processes are spatially explicit across a 20m×20m reef surface and occur at the level of coral individual. Graphics: IAN image library and YM Bozec.

To model spatially realistic reef dynamics across the entire Reef, the model was extended to integrate multiple coral populations within their spatial context of disturbances. Each reef of the Great Barrier Reef marine park (3,806 reef polygons) is represented by a 20m × 20m grid lattice to simulate coral demographics in response to coral's fluctuating environment (temperature, water quality) and exposure to acute stress (cyclones, extreme heatwaves, river runoffs, crown-of-thorns starfish outbreaks). Reef populations are connected through connectivity matrices of larval dispersal of coral and crown-of-thorns starfish (Hock et al. 2014, 2017) and subject to water quality forcing as predicted in space and time by the eReefs modelling platform (Chen et al. 2011, Herzfeld et al. 2016). The model is spatially explicit in three ways: first by simulating the demographic processes of individual coral colonies and crown-of-thorns starfish populations on a reef landscape, second by linking coral and crown-of-thorns starfish demographics to their ambient environment (water quality on a given reef and exposure to cyclones and thermal stress), and third by connecting reefs in a network that represents inter-reef larval exchanges for both crown-of-thorns starfish and corals.

B2.1.1 Coral metapopulation dynamics

Larval connectivity

Dispersal of coral and crown-of-thorns starfish larvae was simulated to determine the connectivity relationships among 3806 individual reefs in the region (Hock et al. 2017). Briefly, larval dispersal was initialised by releasing the particles at the assumed dates of mass coral spawning across the Reef. Dispersal of larvae released in the water column was simulated with the Connie particle tracking tool (Condie et al. 2012), www.csiro.au/connie2/) which uses the same hydrodynamic model as eReefs to generate a three-dimensional model of particle dispersal driven by ocean circulation. This model has hourly time steps and a spatial resolution of hydrodynamic forces over a 4km grid. Larvae that came within 1km of a reef polygon during dispersal would then contribute recruits to that reef, and these recruits were added to the population dynamics models on that reef. The strength of connection between a source and a sink was determined by the number of larvae that reached another reef. This was further modified to represent time-sensitive survival

and development characteristics of the modelled species (Connolly and Baird 2010, Pratchett et al. 2014, Hock et al. 2017), with the probability that a particle would successfully contribute to larval supply at a sink reef dependent on time between spawning and arrival at the sink reef. The simulation of larval dispersal was repeated for designated spawning times over the six years for which the hydrodynamic models were available: summers of 2010-11, 2011-12, 2012-13, 2014-15, 2015-16, and 2016-17 (see below).

Larval supply and recruitment

On a given reef, corals produce offspring following an allometric relationship between colony size and fecundity (Hall and Hughes 1996). The number of larvae is extrapolated to the reef area before dispersion. Retention and larval transport allow estimating of a pool of incoming larvae (L) per unit of reef area, per reef, which represents the amount of coral larvae available for settlement on that reef. With a six-month time step, the model cannot capture the detailed dynamics of larval settlement and post-settlement processes that operate during the early phases of coral ontogeny. Here, these processes are implicitly combined to result in the establishment of six-month-old recruits, which is the assumed age of corals that successfully passed through the suite of demographic bottlenecks (Doropoulos et al. 2016) and survived at the end of the summer step (broadcast spawning occurs at the beginning of summer). Assuming recruitment is density-dependent (e.g. due to compensatory mechanisms affecting the survival of larvae in the water column and settlers on the reef), the number of six-month-old recruits ($N_{recruits}$) is a sigmoid function of the available pool of larvae L:

$$N_{recruits} = \frac{\alpha \cdot L}{\beta + L}$$

where α is the maximum density of recruit (asymptote) able to settle and survive in the following six months and β is the stock of larvae required to produce half the maximum settlement. Consecutively, a number of recruits is generated in each $1m^2$ grid cell from a Poisson distribution with settlement event rate λ calculated as:

$$\lambda = N_{recruits} \times A$$

where A is the proportional space available for settlement in a cell (i.e. uncolonised space). This assumes that the probability of recruitment is directly proportional to the cover of substratum that is suitable for settlement (Connell 1997).

Parameters α and β were calibrated against empirical data of juvenile density on natural substrates. With β set to 50 millions larvae per $400m^2$ (i.e. the surface of a reef grid) and coral specific values of α in the range 0.5–2.5 m-2 (0.5 m-2 for arborescent Acropora, 2.5 m-2 for plating and corymbose Acropora, and 1.5 m-2 for the other 3 coral groups), the model predicts juvenile (<50mm diameter) density values in the range 4–10 m-2 consistent with recent Reef observations across a latitudinal gradient (Figure 29, Trapon et al. 2013).

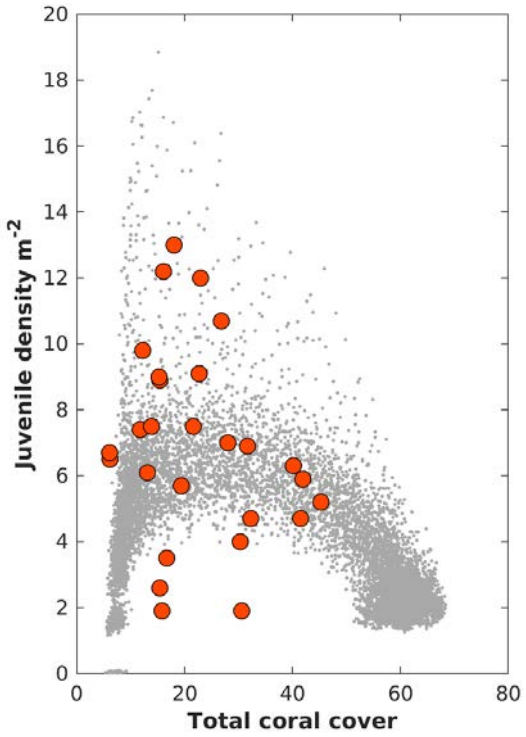

Figure 29: Number of juveniles as predicted by the model (grey dots) and as observed (red dots) by Trapon et al. (2013) over a range of coral reef states. The modelled juvenile densities were obtained by simulating coral recovery from a five percent cover in the Cairns region, thus reflecting changes in coral recruitment with the regional build-up of coral reproductive stock and the concurrent reduction of settlement space.

Post-settlement demographics

Corals enter the model as six-month-old recruits and become juveniles at the next step if allowed to grow (i.e. coral recruitment is processed after all other coral demographic processes, but before disturbances). The growth rate of juveniles is the same for all coral species and fixed to 0.5cm radial extension every six months (Doropoulos et al. 2015, 2016) until they reach a size threshold of 10cm^2 (~3.5cm in diameter), after which they acquire their adult growth rate (Fig. 30A) and survival significantly improves. For example, three-year-old corals of the corymbose/small branching acroporids group would have a diameter of 12.4cm in the absence of partial mortality (Fig. 30B), which falls within the range of observed diameters (7.8–13.7cm) for Acropora millepora at this age by (Baria et al. 2012) in the Philippines.

At this size threshold of 10cm^2, the minimum age is ~two-years-old (i.e. if no partial mortality event has occurred yet) and corals have escaped the most severe post-settlement bottlenecks (Vermeij and Sandin 2008, Doropoulos et al. 2016). Mortality until the 10cm^2 size threshold was fixed to 0.1 per six months which corresponds to the average mortality recorded for 1cm diameter classes in the range 1–4cm on a reef slope at Heron Island (Doropoulos et al. 2015).

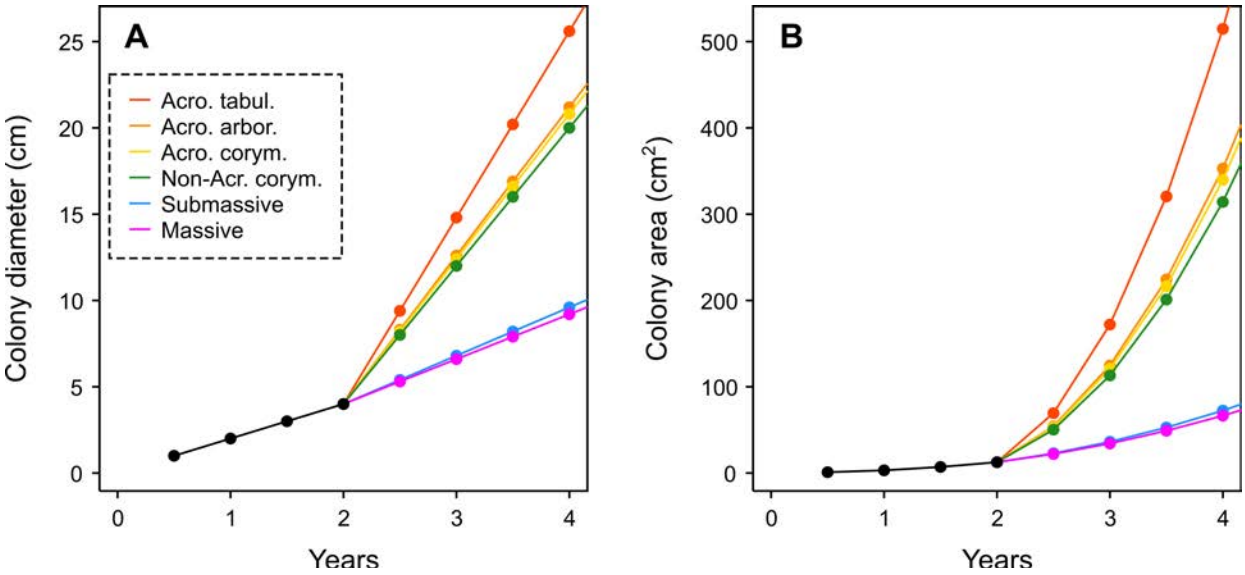

Figure 30: Post-settlement growth of the six modelled coral groups showing theoretical change in colony diameter (A) and colony area (B) within four years post-settlement. Corals are modelled from the stage of recruit (six-months-old) and growth by 0.5cm radial increment every six months until they reach a size threshold of 10cm^2 (~3.5cm in diameter, ~two-year-old recruits) where they acquire their adult growth rate. This size threshold is also use for switching mortality rate from 0.1 to 0.02 per six months.

B2.1.2 Water quality

Nutrients, sediments and other pollutants run off from river catchments and episodically expose coral reefs to varying loads over varying spatial extents and timeframes (e.g. following extreme rainfall and river flood events). To capture these dynamics, exposure to run-off was assessed using the eReefs modelling platform developed by CSIRO. The eReefs coupled physical biogeochemical model considers a range of physical (meteorological, river and wave forcing), sediment (sinking, re-suspension etc.) and biogeochemical (plankton dynamics, benthic productivity, re-mineralisation, de-nitrification etc.) processes to simulate water quality (Robson et al. 2013, Herzfeld et al. 2016, Baird et al. 2017). To model the effects of changing water quality in time and space on coral and crown-of-thorns starfish dynamics, we used the retrospective daily predictions of suspended sediments and chlorophyll at 4km × 4km resolution with the best available forcing provided by model configurations GBR4_H2p0_B2p0_Chyd_Dcrt (12/2010–10/2016) and GBR4_H2p0_B2p0_Chyd_Dnrt (11/2016–12/2017). Suspended sediment concentrations (SSC) were obtained by summing together the spatial layers of Mud, CarbSand (carbonate sand) and FineSed (fine sediment) representing small-sized re-suspending particles of different optical properties and origin. While Mud and CarbSand describe re-suspending particles from the deposited sediments, FineSed tracks the particles entering the Reef through river catchments.

Impacts of suspended sediments on coral demographics

For modelling coral demographics, we focus on suspended sediment concentrations (SSC) predicted at different depths over different seasons. Suspended sediment influences many aspects of coral biology (Anthony et al. 2009, Jones et al. 2015) but are only considered here at the early life-history stages of broadcast spawner corals: (i) fertilisation followed by embryo development before transportation of coral larvae off the reef (hereafter referred to as “reproduction success”), (ii) survival of corals recruits within six months following settlement, and (iii) growth of coral juveniles. Spatio-temporal predictions of coral reproduction and recruitment success were obtained by combining maps of suspended sediments with dose-response curves derived from recent experimental Great Barrier Reef data (Humanes et al. 2017b, 2017a).

Using *Acropora tenuis* as a model species, Humanes et al. (2017b) assessed in tank experiments the effects of SSC, temperature and nutrient concentrations on fertilisation success, embryo development, larval development and settlement success. In a first experiment, they demonstrated an effect of increasing SSC (0, 5, 10, 30 and 100 mg.L-1) on the proportion of fertilised eggs (~1.5 hours after fertilisation) while nutrient concentrations and temperature had no or little impact. A dose-response curve of fertilisation success to SSC can be obtained by fitting a simple linear model to the proportion of fertilised eggs across all SSC and nutrient treatments at ambient temperature (Fig. 31A). In a second experiment, Humanes et al. (2017b) exposed embryos (eight-hour-old) to increasing SSC, nutrients and temperature, until they became ciliated larvae (~36-hour-old). Coral larvae were then maintained in controlled conditions without any stressor and the proportion of settled larvae was recorded after 24 hours of induced settlement. While early (embryo) stress exposure did not affect survival to the settlement stage, larval settlement success responded significantly to all stressors, with SSC having the strongest effect. Here, SSC treatments were combined with the low and medium nutrient treatment at ambient temperature to fit a dose-response curve of relative settlement success (Fig. 31B). No significant effects of SSC were observed after exposure at later development stages. Finally, the two response curves were combined into a single one that predicts the relative success of coral reproduction as a composite function of fertilisation success and future capacity (i.e. competency) to settle (Fig. 31C). This function can be used to estimate the number of competent larvae produced on a reef exposed to SSC during spawning events (i.e., prior to dispersion).

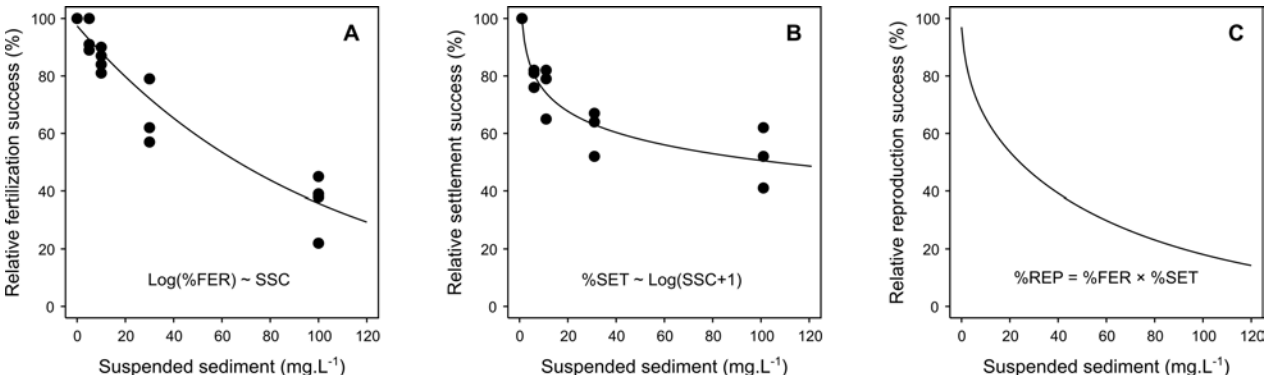

Figure 31: Modelling of dose-response relationships of coral pre-settlement processes to concentrations of suspended sediment (SSC) from experimental observations (Humanes et al. 2017b). (A) Experimental data (dots) of relative fertilisation success (percent fertilised eggs relative to control) fitted with a linear model (R2=0.88, n=20). (B) Experimental data (dots) of relative settlement success (percent settled larvae relative to control) following exposure of embryos to increasing SSC, fitted with a linear model (R2=0.88, n=15). (C) Empirical response curve of percent 'reproduction success' as the combined success of gamete fertilisation and development of competent larvae relative to reef waters devoid of suspended sediments (i.e. on reefs where SSC = 0 mg.L-1).

Spawning corals release combined egg-sperm bundles that immediately ascend to the surface (Richmond 1997, Jones et al. 2015). Gamete bundles then break apart within an hour and fertilisation takes place near to the surface, with first cleavage generally occurring within six hours. To capture sediment exposure at these early (<36-hr) development stages of broadcast coral larvae, daily spatial predictions of near-surface (-0.5m) SSC were extracted from eReefs at the assumed dates of mass coral spawning across the Reef. Spawning dates between 2011 and 2016 (C. Doropoulos, CSIRO, pers. comm.) account for consecutive (split) spawning events and patterns of synchrony across the northern, central and southern regions. From the assumed spawning date in a given region, the 4km × 4 km pixeled SSC values were averaged over three consecutive days to account for spatio-temporal variations in spawning synchrony and embryo development. The resulting mean SSC values were further averaged over multiple spawning

events (Fig. 32A). Predictions of coral reproduction success were calculated for each pixeled SSC and assigned to the nearest reef polygon, thus enabling the mapping of reproduction success at a reef-by-reef scale (Fig. 32B).

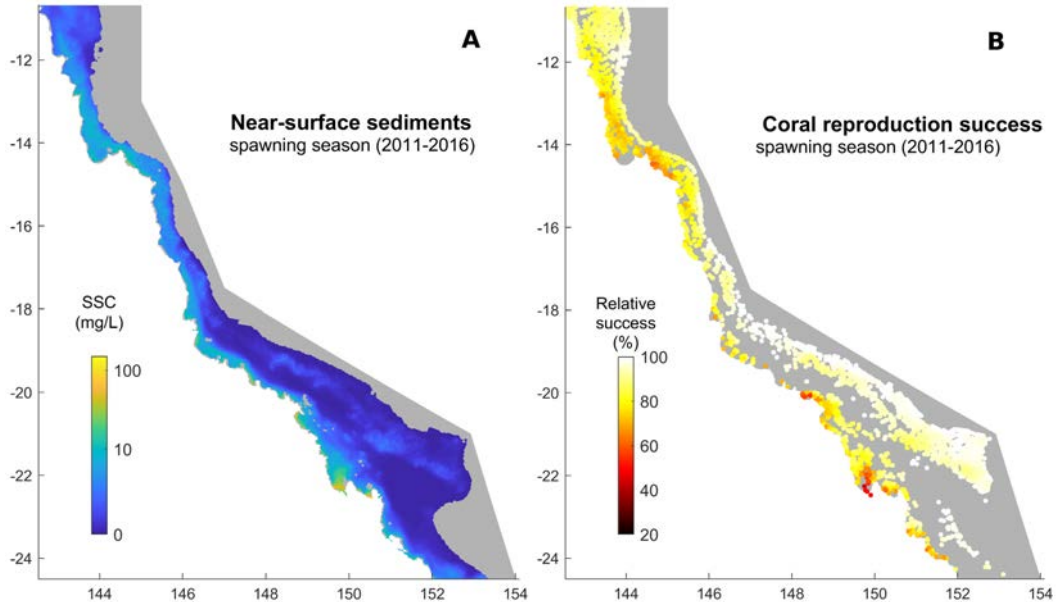

Figure 32: Great Barrier Reef 2011–2016 mean predictions of (A) near-surface suspended sediment concentrations (SSC) at 4km ×4km resolution during mass coral spawning (note the logarithmic scale) and (B) relative success of coral reproduction at 3806 reef centroids (dots) inferred from SSC using the empirical relationship shown on Fig. 31C.

Suspended sediments also affect the early-life history of corals after dispersion and settlement. In another series of experiment Humanes et al. (2017a) assessed the impacts of increasing SSC on the growth and survival of three- to six-month-old recruits of three corymbose/small branching corals: Acropora tenuis, Acropora millepora and Pocillopora acuta. After 40 days of exposure to crossed treatments of nutrients and SSC, a significant effect of SSC was detected on the survival of A. millepora recruits, but not on the other two species; nutrient concentrations had no significant effect on any species. Here, SSC treatments at low and high nutrient concentrations were combined to fit a dose-response curve of the survival of Acropora recruits relative to baseline (null SCC) treatments (Fig. 33A). For the sake of simplicity, we assumed that one dose-response curve can fit all species (Fig. 33B).

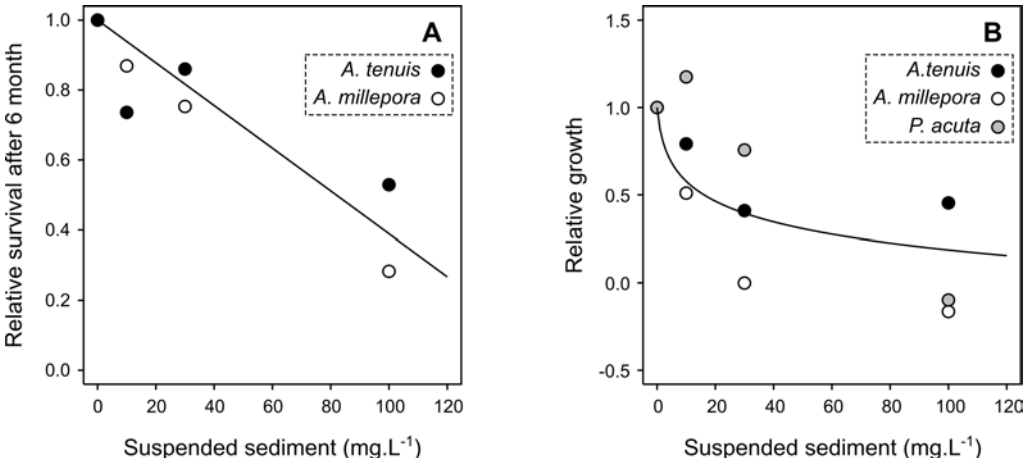

Figure 33: Modelling of dose-response relationships of post-settlement survival and growth following exposure to suspended sediment concentrations for 40 days based on the experimental data (dots) of (Humanes et al. 2017a). (A) Relative survival (survived fraction relative to control, here extrapolated to 6 months) of three- to six-month-old coral recruits following sustained exposure to SSC fitted with a linear model (R2=0.89, n=8). (B) Proportional growth of coral recruits relative to control following exposure of embryos to increasing SSC (log-transformed), fitted with a linear model (R2=0.79, n=12).

Exposure of *Acropora* recruits (i.e. 1cm^2 corals) to suspended sediment across the Reef was captured from eReefs daily predictions of SSC (4km × 4 km pixel) at mid-depth (~ -6m) during the 2011-2018 summer months (November to April, Fig. 34A). An estimate of recruit survival was produced for each daily value of pixeled SSC from the empirical dose-response described above (after downscaling to daily survival). Predicted daily survivals were combined over each summer period and assigned to the nearest reef polygon. This resulted in six spatial layers (one for each recruitment season between 2011 and 2016) of six-month cumulative survival of *Acropora* recruits at a reef-by-reef scale (Fig. 34B).

Similarly, spatial layers predicting the growth potential of coral juveniles (i.e. below 2.5cm diameter) were derived by averaging the pixeled SSC values in summer (six months from November to April) and winter (six months from May to October) for every year of the 2011-2016 period (Fig. 34C). Pixeled predictions of relative juvenile growth (all coral species) were assigned to the nearest reef polygon (Fig. 34D).

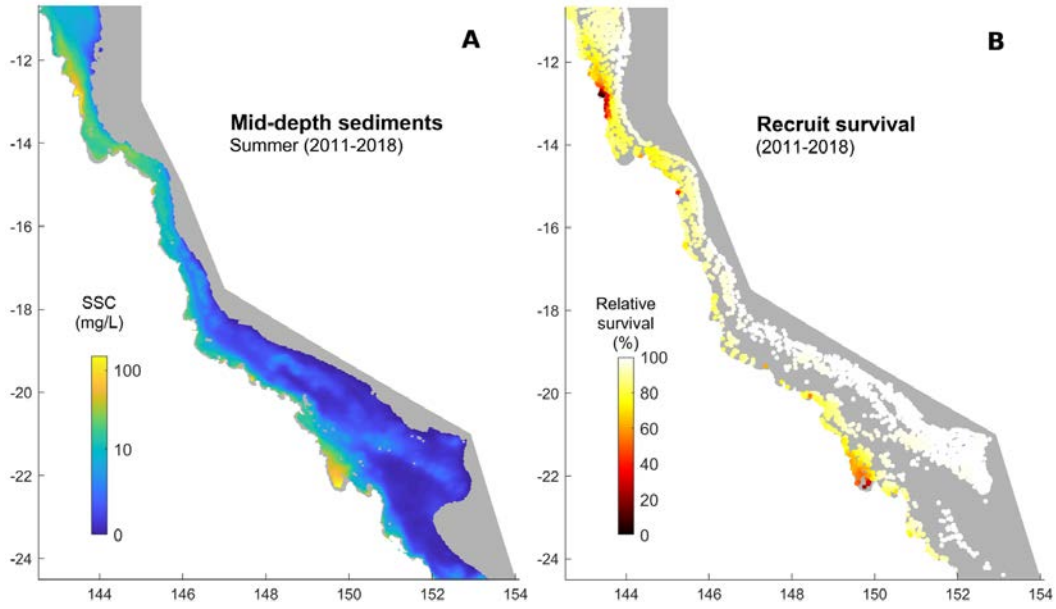

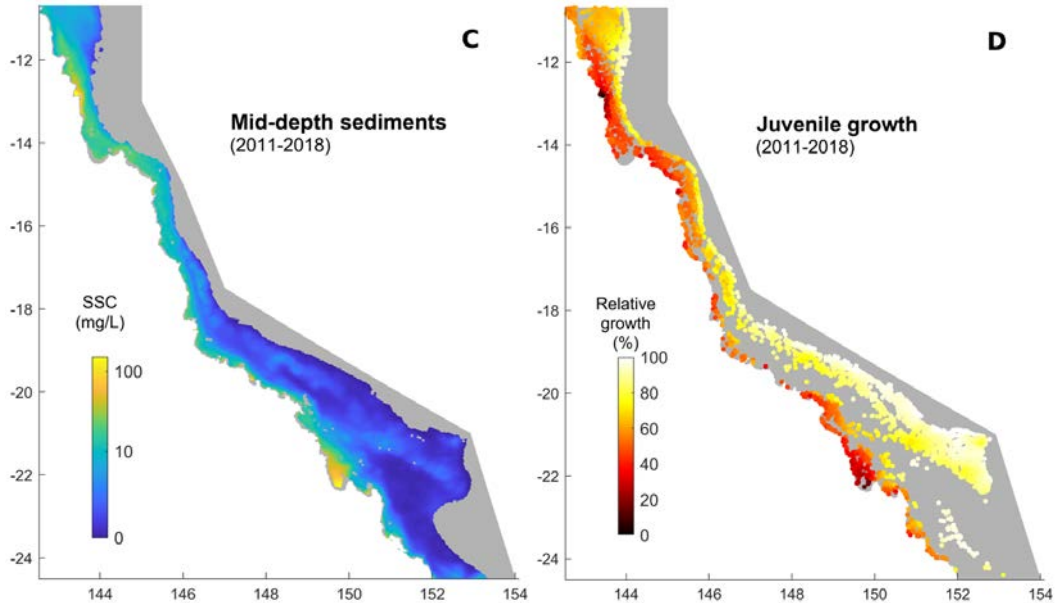

Figure 34: Great Barrier Reef 2011–2018 mean predictions of suspended sediment concentrations (SSC) and impacts on coral post-settlement demographics. (A) Mid-depth (~ -6m) SSC during summer months averaged from November to April over the 2011–2018 period (note the logarithmic scale) and (B) corresponding reef-by-reef predictions (dots) of relative survival of Acropora recruits within six months of settlement (survival of other corals assumed to be insensitive to SSC). (C) Mid-depth (~ -6m) SSC averaged over each season and year (note the logarithmic scale) and (D) corresponding reef-by-reef predictions of relative growth of coral juveniles (all coral species).

Impacts of chlorophyll concentrations on crown-of-thorns starfish demographics

Concentrations of total chlorophyll a (Chla) at 4km × 4km resolution were extracted from eReefs between 2011 and 2016 during the spawning season of crown-of-thorns starfish. Daily maximum Chla concentrations from December to January were used as predictors of the relative survival of crown-of-thorns starfish larvae before dispersal following Fabricius et al. (2010).

B2.1.3 Crown-of-thorns starfish outbreaks dynamics

Outbreak dynamics of the crown-of-thorns starfish (Acanthaster planci, crown-of-thorns starfish) are simulated using a simple cohort model (Fig. 35). The model is structured by age (six-month age classes) and integrates age-specific rates of mortality (Fig. 36) fecundity and coral consumption (e.g. Kettle and Lucas 1987, Keesing and Lucas 1992). crown-of-thorns starfish release their gametes in summer (December-January) and the resulting number of larvae is affected by the ambient concentration of chlorophyll a (Chl-a) as predicted by eReefs. High chlorophyll concentrations promote the survival of crown-of-thorns starfish larvae (Fabricius et al. 2010) and connectivity information (Hock et al. 2014) determines the amount of crown-of-thorns starfish larvae that are retained or distributed to other reefs. The stock of crown-of-thorns starfish larvae that is available for settlement on a given reef is thus a function of local retention and external supply. The amount of corals consumed varies between coral species, and when coral cover drops below five percent the population of coral-feeding crown-of-thorns starfish dies due to starvation.

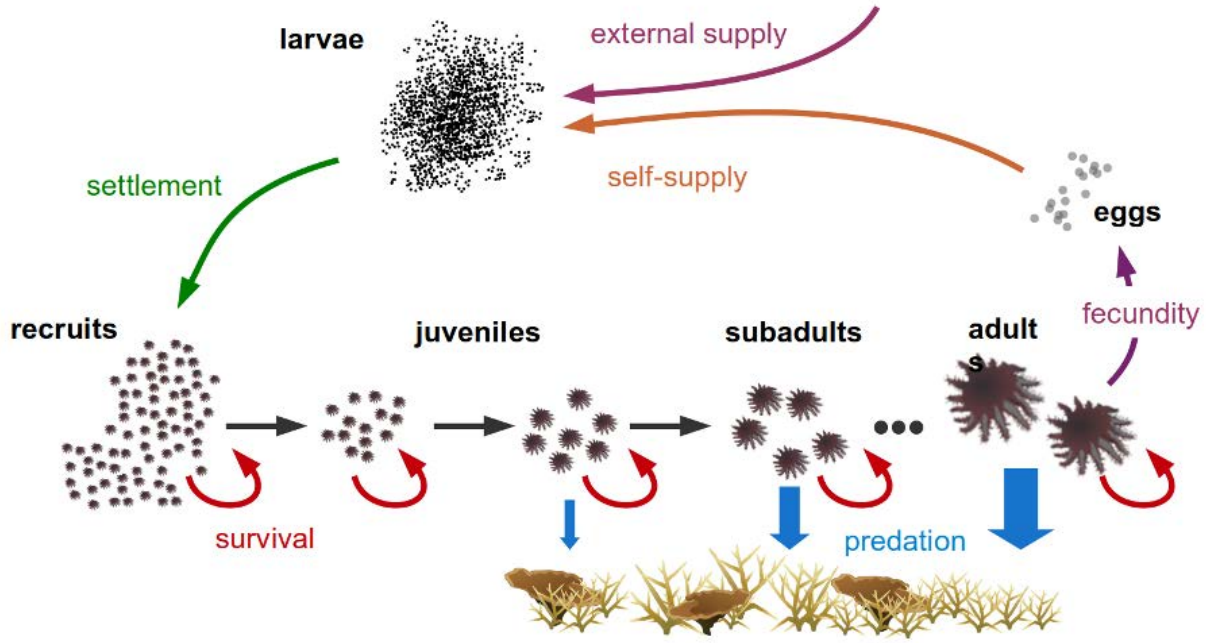

Figure 35: Modelling of crown-of-thorns starfish population dynamics and impact on corals with the demographic processes parameterised using empirical data. The model describes the fate of crown-of-thorns starfish cohorts recruiting in summer and subject to size-specific survival during their life. Settlement occurs from a pool of larvae that results from the retention of locally produced offsprings and the incoming of larvae from connected reef populations. Individuals in one year+ cohorts feed on corals at size-specific consumption rates.

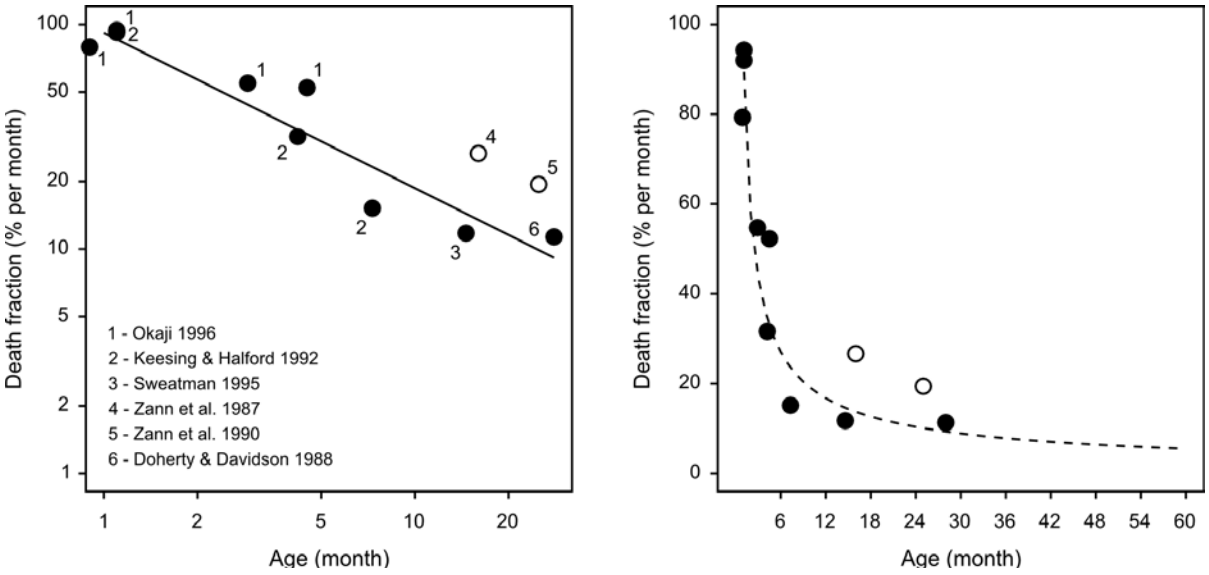

Figure 36: Point estimates of crown-of-thorns starfish mortality (monthly death fraction) as a function of age (right) and log-log relationship (left). Mortality estimates are based on survival rates scaled to one month. Age represents the median age of the cohort during the study period. Empty circles denote estimates excluded from the model due to the prevalence of disease (Zann et al. 1987) and low accuracy in abundance estimates (Zann et al. 1990). Model statistics: n = 8, intercept significantly non null at p<10-7, slope significantly non null at p<10-4, adjusted R2 = 0.89.

B2.1.4 Cyclones

Whole-colony and partial mortality of adult coral colonies is a function of colony size and storm strength (Edwards et al., 2011, Bozec et al. 2015), with group-specific adjustments to account for the sensitivity of the different growth forms: ×10 for arborescent Acropora, ×8 for plating and corymbose/small-branching corals, ×1 for massive and encrusting forms. Scouring by sand during a cyclone causes 80 percent whole-colony mortality in recruit and juvenile corals (Mumby, 1999).

B2.1.5 Widespread coral bleaching

Widespread coral bleaching on the Reef is assumed to be primarily driven by thermal stress (Berkelmans 2002, Hughes et al. 2017, 2018). Bleaching only occurs during summer steps following exposure maps to thermal stress based on past records (detailed in section “hindcast”), or forward projections of sea surface temperature (sea surface temperature) anomalies predicted under different warming scenarios by global climate models (detailed in section “forecast”). Coral mortality following bleaching events is a function of thermal stress (degree heating weeks) parameterised with bleaching mortalities reported during the 2016 bleaching event recorded across the Reef by Hughes et al. (2018). While this study provides one of the most comprehensive records of bleaching mortalities on corals from the Great Barrier Reef, there are few limitations: (1) Hughes et al. (2018) only recorded coral mortality at the peak of the bleaching event (over two to three weeks in March 2016), i.e. initial mortality, likely to underestimate coral mortality experienced over the entire bleaching event; (2) that the survey of bleaching mortality was performed at 2m depth, likely to overestimate any extrapolation to deeper corals; (3) that no information is available on partial mortality (i.e. only whole-colony mortality was recorded at the peak of the bleaching event), likely underestimating coral damages during the 2016 bleaching event. While a number of assumptions are required to parameterise realistic bleaching-induced mortalities, including per capita mortality rates, rates of incidence of partial mortality and extent of tissue lost due to bleaching, the observations of coral cover loss of Hughes et al. (2018) six months after the bleaching event can be used for calibration.

B2.1.6 Whole-colony mortality

An empirical relationship between coral mortality and thermal stress (degree heating weeks) was derived by regressing Hughes et al. (2018)’s observations of initial coral mortality (whole-colony mortality) against their satellite-derived 5km resolution degree heating weeks values. This simple linear model allows generating deterministic (Fig.37) or stochastic predictions (i.e. falling within the confidence intervals of predictions) of bleaching mortality for any degree heating weeks value. In the model, bleaching mortalities are generated only when thermal stress is equal or above 4°C-weeks to avoid excessive bleaching mortality at low thermal stress.

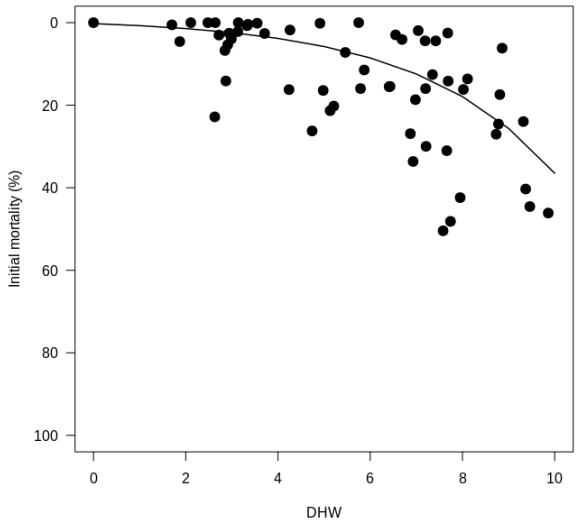

Figure 37: Initial coral mortality (dots) recorded at the peak of the 2016 bleaching events by Hughes et al. (2018) in the northern Great Barrier Reef, fitted with a linear model (modelled variable is log(mortality+1), R2=0.45).

B2.1.7 Extent of partial mortality due to bleaching

Baird and Marshall (2002) found almost no partial mortality on A. hyacinthus and A. millepora during the 1998 bleaching event on the central region of the Reef (Palm Islands Group). Consequently, the extent of partial mortality was considered minimal and fixed to five percent of colony area for the three Acropora groups (i.e. plating corals, arborescent corals and corymbose/small branching acroporids) as well as for the pocilloporid/other non-acroporid corymbose group. For small massive/submassive and large massive coral groups, this value was set respectively to 40 percent and 20 percent of colony area based on their observations on Platygyra daedalea and Porites lobota.

B2.1.8 Species-specific sensitivity to bleaching

Mortality of each coral group was further adjusted using the information on initial mortality per taxa reported by Hughes et al. (2018). Taking as a baseline an average mortality of ~20 percent across taxa, relative mortalities were estimated for each group as follows: (1) plating corals: 1.6; (2) arborescent (staghorn) corals: 1.5; (3) corymbose/small branching acroporids: 1.4; (4) pocilloporids and other non-acroporid corymbose: 1.7; (5) small massive/submassive/encrusting corals: 0.25; (6) large massive corals: 0.25.

B2.1.9 Incidence of partial mortality due to bleaching

While the study of Hughes et al. (2018) does not provide specific information about bleaching-induced partial mortality, different incidence values (i.e. the probability that a given coral exhibits partial mortality) were tested in an attempt at matching the observed losses of coral cover reported by Hughes et al. (2018). For a given thermal stress (degree heating weeks), the incidence of partial mortality is obtained by multiplying the predicted whole-colony mortality by a constant C, assuming the incidence of partial and whole-colony mortalities are correlated.

Calibration

With a value of C = 5 (i.e. the incidence of partial mortality is five times the incidence of whole-colony mortality), model simulations were able to reproduce the range of coral cover loss reported by Hughes et al. (2018) after the 2016 bleaching event (Fig. 38). This calibration was

performed by simulating the impact of the 2016 bleaching for hypothetical reefs initialised with coral cover values reported by Hughes et al. (2018) before bleaching. Coral cover was dis-aggregated among the six functional groups with a community composition assumed to be representative of an outer reef of the region (following AIMS Long-term Monitoring Program for the Cairns region). Thermal stress was stimulated by randomly exposing reefs to the recorded 2016 degree heating weeks values.

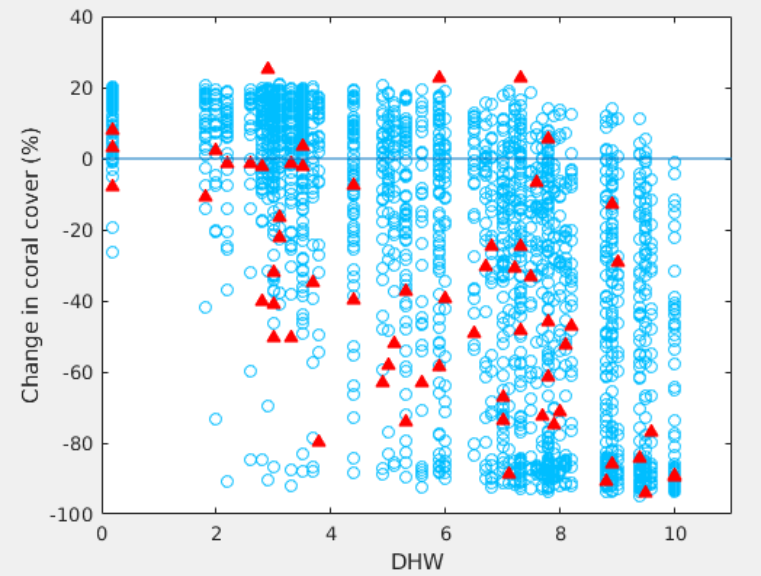

Figure 38: Stochastic predictions of coral mortality (empty blue dots) based on the degree heating weeks values observed during the 2016 bleaching, with the observations (red triangles) of Hughes et al. (2018).

B2.1.10 Rubble

Extensive coral mortality following acute disturbances (cyclones, bleaching and crown-of-thorns starfish outbreaks) generate loose coral debris that cover the reef substratum and inhibit coral recruitment (Dollar and Tribble 1993, Fox et al. 2003, Biggs 2013). The percent coral cover lost is transformed into percent rubble cover with a conversion factor of 1.5 (e.g. a loss of 20 percent coral cover produces 30 percent rubble cover) in order to account for the greater surface covered by collapsed skeletons relative to their living counterparts. Coral rubble is generated immediately after cyclones, but only three years after bleaching and crown-of-thorns starfish predation (Sano et al. 1987) to delay the structural collapse of dead skeletons relative to erosion. Assuming coral recruits do not survive on loose rubble (Fox et al. 2003, Viehman et al. 2018), the rate of juvenile survival at a given time step (0.9 per six months without suspended sediments) is reduced proportionally to the area covered by rubble. For example, with 30 percent rubble cover, the survival rate of juveniles becomes 0.9 × (1 – 0.3) = 0.63 per six months.

Loose coral rubble tends to stabilise over time due to natural processes of binding and cementation (Rasser and Riegl 2002). We modelled these dynamics using a simple exponential decay function with the assumption that 50 percent of rubble is stabilised over four years. This rate is a conservative estimate of the observed dynamics of experimental rubble stabilisation in Curaçao, Netherlands Antilles (Biggs 2013). In two reef sites, Biggs (2013) followed ~20 piles of fragments of branching Acropora (Fig. 39A) over four years, recording the number of piles stabilised by turf algae in at least one survey (‘temporary’ stabilisation). Several coral recruits were detected on the stabilised piles, suggesting that coral settlement and survival is possible during the early stages of rubble consolidation in relatively calm hydrodynamic environments. In the model, rubble stabilisation can be delayed with the addition of new coral fragments following coral mortality events. The area of rubble newly stabilised becomes epilithic algal matrix (i.e. carbonate substratum suitable for coral settlement) and increases proportionally the survival of

coral juveniles. For example, the stabilisation of 20 percent of rubble covering 30 percent of the reef substratum increases juvenile survival from 0.63 per six months to
$0.9 \times (1 - (0.3 - 0.3 \times 0.1)) = 0.68$ per six months.

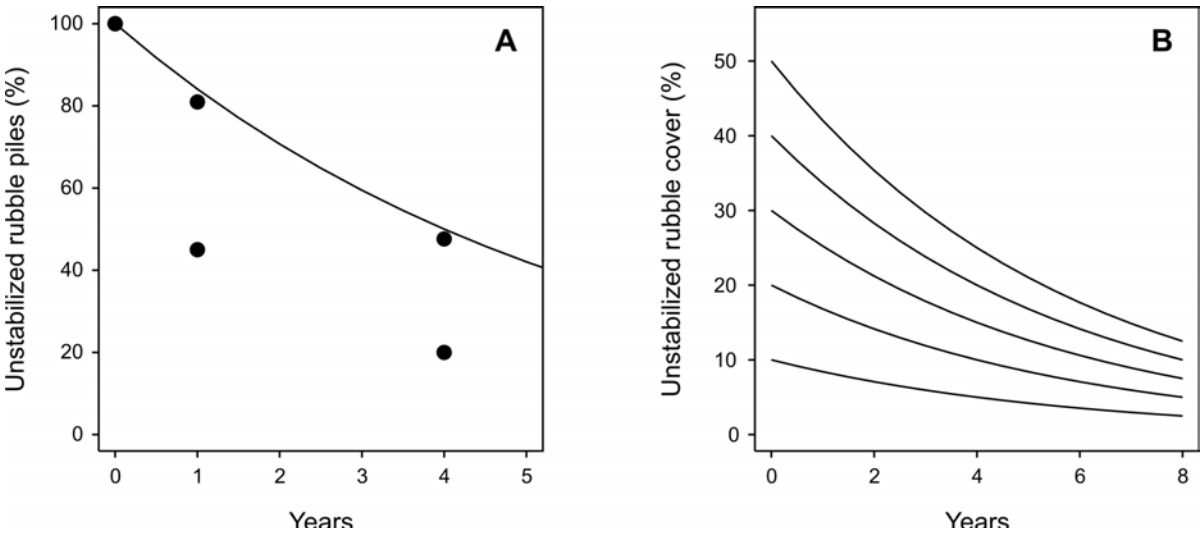

Figure 39: Modelling of rubble natural stabilisation. (A) Proportion of experimental rubble piles (dots) showing no sign of stabilisation over the course of Biggs (2013)'s in situ experiment fitted with an exponential decay function.

B2.1.11 Genetic adaptation

The model accounts for the evolutionary dynamics of coral fitness to temperature change by integrating a quantitative genetic model of thermal tolerance and adaptation. Phenotypic tolerance to increasing sea surface temperature was implemented following the polygenic model developed by Matz et al. (2018). Briefly, thermal tolerance of a coral colony is shaped by a set of quantitative trait loci that are transmitted from parents to offspring. Each thermal quantitative trait locus is associated with an effect size (in °C) and the sum of effect sizes over all loci gives the breeding value for thermal tolerance (Fig. 40). The actual phenotype is obtained by adding a normally distributed random noise to the breeding value to model imperfect heritability. This sets a specific phenotypic optimum (Topt) to every coral from which thermal fitness can be calculated relative to the ambient temperature.

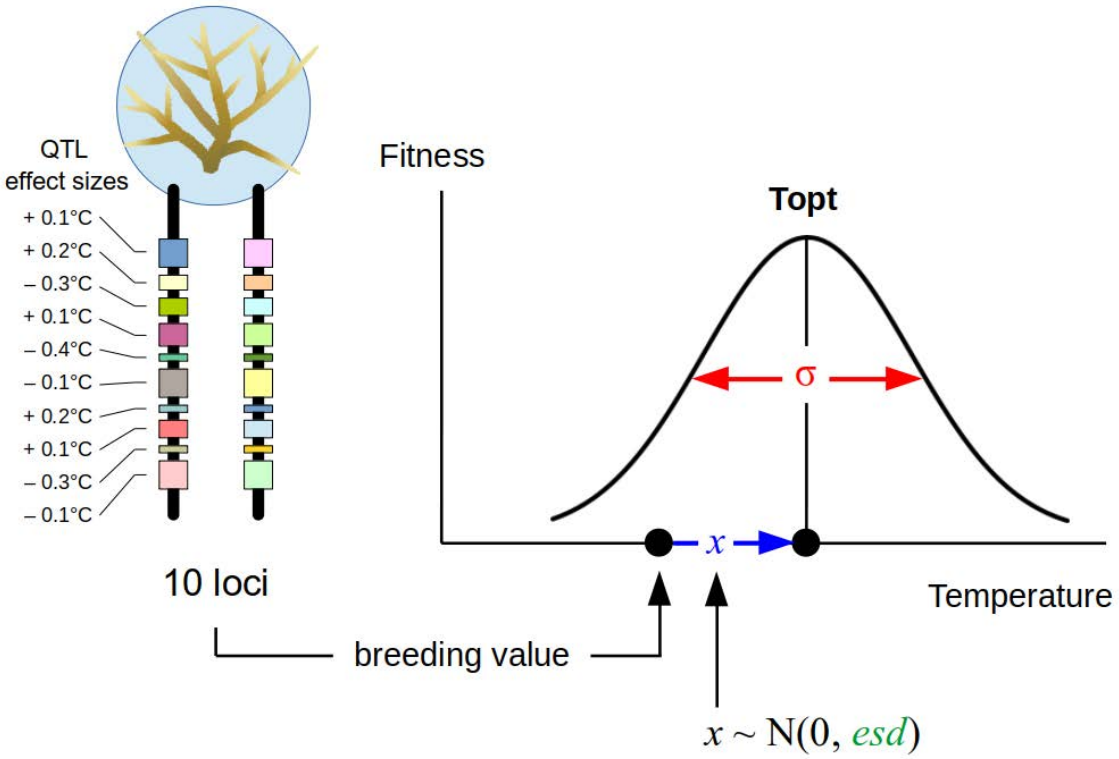

Figure 40: Modelling of thermal adaptation. Coral fitness to temperature is determined by a set of quantitative trait loci (QTL) each having a small quantitative effect (positive or negative) on thermal tolerance. For every coral individual, the sum of quantitative trait loci gives the breeding value for thermal tolerance, on which a normally distributed random noise x (blue) is added to obtain the phenotypic thermal optimum Topt. The value x represents the environmental component of the phenotypic Topt and relates to the heritability of thermal tolerance: the greater the noise the lower heritability. Thermal fitness is maximal when the ambient temperature perfectly matches the coral Topt, thus conferring a demographic advantage to the coral (growth, reproduction). Two parameters drive the efficiency of genetic adaptation: (1) the standard deviation σ (red) of the Gaussian curve that controls the slope of the fitness decline (tolerance breadth) and (2) the standard deviation esd (green) of the normally distributed random noise x.

Model burn-in: Creation of genotypes pre-adapted to warming

Model simulations start for each reef grid with an equilibrial stock of quantitative trait loci pre-adapted to warming and assumed to be representative of the genetic diversity of standing populations. This stock is generated behind-the-scene by running a model of coral generations similar to Matz et al. (2018) over two burn-in periods. The first period allows creation of a genetic stock at equilibrium with no warming by simulating 100 generations of 10,000 corals under stationary sea surface temperature. At initialisation, quantitative trait loci are created by generating random values following a normal distribution (mean=0, SD=σ). As in Matz et al. (2018), thermal tolerance is assumed to be an expression of two alleles of 10 loci, so that 20 loci are assigned to each coral at random. The associated Topt is calculated by adding a normally distributed scalar (mean 0, SD=esd) to the breeding value (sum of the 20 loci). At each generation step, sea surface temperature fluctuates randomly (mean 0, SD=0.025) and fitness of all coral individuals is calculated from the difference between Topt and sea surface temperature. Fluctuating temperatures affect coral reproduction: gamete production is proportional to fitness with perfectly fit corals producing a maximum 100 gametes. Each gamete is created through a random selection of 10 of the 20 parental loci, with mutations occurring at a rate of 1*e*-six per locus. A mutation results in the addition to the muted locus of a scalar generated from a normal distribution (mean 0, SD=0.2) (Matz et al. 2018). Fertilisation occurs through the random selection of two gametes given they come from different parents (i.e. self-fertilisation is not allowed) and leads to the creation of a new phenotype. At each generation, 10,000 new

genotypes are created to maintain constant population size. At the end of the equilibration period, another 100 generations are simulated with sea surface temperature increasing at a rate of 0.05°C per generation (~0.1°C per decade, assuming a coral generation represents ~ five years, Matz et al. 2018) in order to obtain a genetic pool of quantitative trait loci pre-adapted to warming.

Initialisation of demographic simulations

Demographic simulations start with the creation of coral colonies of different sizes (i.e. circular areas in cm^2) following a lognormal distribution, so that the total area of live coral matches the input value of proportional cover for each coral species. Coral colonies are randomly dispatched over the grid and assigned a genotype randomly selected from the local pool of quantitative trait loci. Phenotypes are then computed as breeding value plus the Gaussian distributed noise plus the mean sea surface temperature calculated for each reef over the past 10 years, assuming this represents the average value of Topt across the population. Corals keep the same Topt during their entire life and thermal tolerance is expressed by separating responses to chronic temperature fluctuations (mean annual sea surface temperature) and to episodes of marine heatwaves (degree heating weeks). This allows for the simulation of the evolutionary dynamics of corals through the combined 'soft' and 'hard' selection of thermal tolerance. Processes underlying a soft selection involve colony growth and fecundity as an expression of coral fitness. Hard selection is achieved through resistance to bleaching, with coral survival being dependent on degree heating weeks values relative to Topt.

Coral fitness in response to fluctuating sea surface temperatures

At every time step, thermal fitness is evaluated for each coral by calculating the difference between Topt and the mean annual sea surface temperature of the reef, with thermal fitness declining away from Topt for warmer and colder temperatures. A drop-in fitness reduces growth and fecundity proportionally. Available experimental evidence is quite limited for a robust parametrisation of the shape of this curve across the full range of temperature fluctuations (Fig. 41A,B). As a first approximation, one can assume coral fitness follows a Gaussian curve (Matz et al. 2018) so that change in fitness is symmetrical when temperature moves away from Topt on the warm and cold sides. An important parameter is the standard deviation σ of this Gaussian curve as it determines the breadth of thermal tolerance. While σ is likely to vary among coral species, the existing data are limited and somewhat conflicting, leading Matz et al. (2018) to explore a range of values from 0.5 to 2 corresponding, respectively, to a fitness drop of 86 percent and 13 percent when temperature mismatches Topt by 1°C (Fig. 41C). With a limited empirical support, predicting the evolutionary dynamics of corals is challenging and requires simulating adaptation scenarios with different tolerance breadth values.

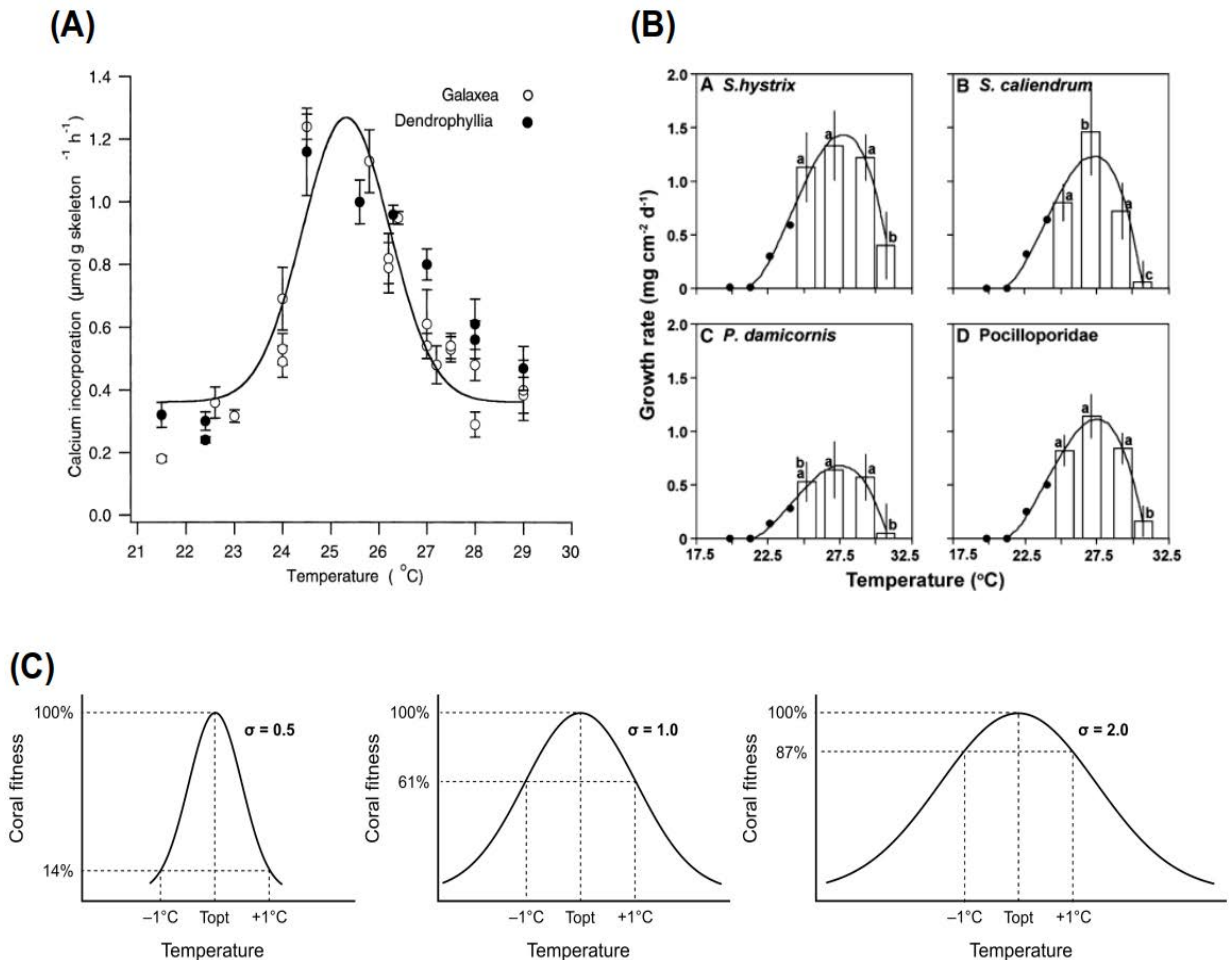

Figure 41: Experimental growth curves of corals subject to a range of temperatures (A) (Marshall and Clode 2004) at Heron Island (southern Great Barrier Reef) and (B) (Edmunds 2005) at One Tree Island (southern Reef). (C) Modelled growth curves with increasing tolerance breadth (σ) values.

While thermal fitness results in the selection of the most tolerant and well-adapted phenotypes to fluctuating temperatures, the success of adaptation to warming is also driven by the efficiency of trait transmission from one coral generation to the next. Phenotypic thermal optima are partly determined by the environmental component which modulates the genetically driven breeding value. Specifically, a strong environmental influence in the expression of thermal tolerance would imply a loose relationship between the phenotypic and genotypic compositions, pointing to a low heritability of thermal traits. Following Matz et al. (2018), heritability is represented by the standard deviation (esd) of the normal distribution used to generate the value of Topt from the breeding value. A null value of parameter esd implies that Topt perfectly matches the breeding value, meaning heritability is perfect; under this scenario, fluctuating temperatures might result in an efficient selection of genes that confer thermal tolerance, leading to a rapid evolution of thermal traits. Conversely, the greater the esd value the greater the chance to generate discrepancies between Topt and the breeding value, which can lead to selecting genes that are not related to the actual fitness of the coral. In this case, the evolution of thermal traits is likely to be slow, although a greater diversity of phenotypes in the population might buffer the selective pressure of increasing temperatures. As for the breadth of thermal tolerance, heritability in the form of esd is largely unknown for corals so that different values must be considered as possible evolutionary scenarios. Matz et al. (2018) explored the dynamics of coral adaptation with esd = 0 (perfect heritability) and esd = 2 (low heritability) which is considered here as the upper and lower bounds of heritability of thermal tolerance in the absence of empirical support.

B2.1.12 Coral resistance to acute thermal stress (bleaching)

The phenotypic expression of thermal tolerance also includes greater resistance to bleaching and it is assumed that sensitivity to extreme temperatures is proportional to Topt, so that warm-adapted corals have greater resistance to bleaching. Marshall and Clode (2004) measured calcification rates in polyps of two coral species, Galaxea fascicularis and Dendrophyllia sp. at Heron Island at different times of the year from 1991 to 2001. They observed a change in calcification with temperature (range 21–29°C) with a maximum calcification rate achieved at ~25°C (Fig. 42A). Monthly averages of maximum temperature recorded at Heron Island from 1995 to 2000 indicated a maximum monthly mean (MMM) temperature of ~28°C, which is approximately +3°C above the optimum temperature estimated for these two corals.

Degree heating weeks, a measure of thermal stress able to cause bleaching mortality, is calculated as the cumulative exposure to temperatures exceeding a critical threshold (Fig.42), which is currently defined as 1°C above a reference MMM (e.g. between 1985 and 1993):

$$T_{critical} = MMM_{85-93} + 1°C$$

Assuming MMM is the functional equivalent of Topt, the amount of thermal stress for a given coral X can be recalculated using a threshold that is function of the coral thermal optimum:

$$T_{critical}(X) = T_{opt}(X) + offset°C + 1°C$$

where the offset corresponds to +3°C following Marshall and Clode (2004). This offset of 3°C is assumed for any coral on any reef in the absence of information across species and latitudes. Therefore, instead of calculating degree heating weeks uniformly for all corals from the MMM of a given reef, degree heating weeks stress is estimated for every coral individually relative to its thermal optimum.

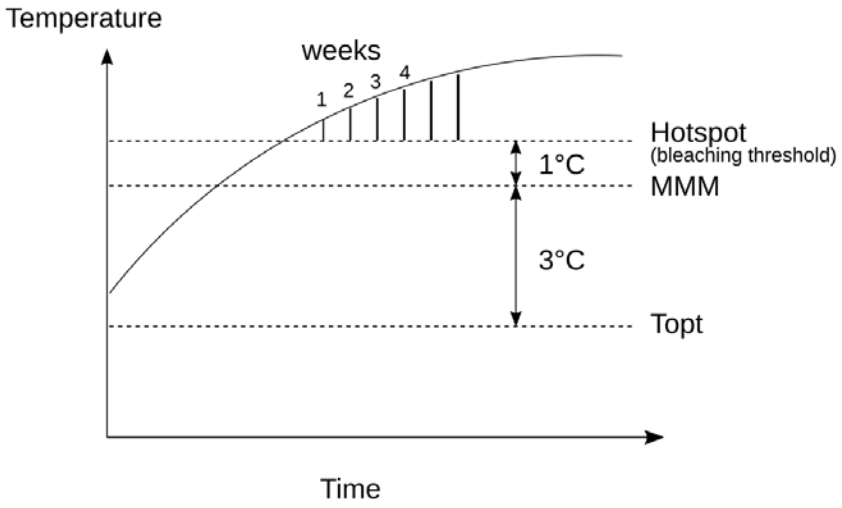

Figure 42: Principle of thermal stress (degree heating weeks) calculation as a function of the optimum temperature (Topt) of each coral.

B2.1.13 Gene transmission through sexual reproduction (mass spawning)

After each reproductive event, a pool of 1000 genotypes representative of the QTL composition of coral offspring is created for every reef. These genotypes are generated through the random sampling of coral parents where the probability of sampling is proportional to thermal fitness and the number of offspring produced by each coral. As a result, corals with a Topt close to the ambient temperature are more likely to pass their genes to the next generation. To reflect the genetic diversity of a given source reef, mutation rate is elevated proportionally to reef area, so that larger reefs have a greater diversity of genotypes due to a greater incidence of genetic mutation. The pools of larval genotypes are used to determine the genetic composition of coral recruiting on a sink reef. Every successful settler is assigned a genotype by sampling randomly

across all the larval genetic pools of donor reefs, with a probability of sampling that is proportional to the contribution of each source reef to larval supply.

B2.1.14 Model outputs

For a given set of parameter values, multiple runs are required to capture the variability resulting from stochastic mortality and spatial interactions. Model outputs include the cover of the six coral groups every six months averaged across multiple replicate simulations, but also the density of coral recruits, juveniles and adults for different size classes in every reef of the Reef, the size distribution of each coral population, the average cover of turf and macroalgae, the average cover of rubble and average crown-of-thorns starfish density at every reef. Mortality events are tracked through coral cover loss associated with each stressor. In addition, estimates of the genetic and phenotypic (thermal optimum) diversity are available at a reef-by-reef scale. Importantly, the model simulates a level of uncertainty associated with the predicted reef state. Some of that uncertainty stems from stochastic processes such as cyclones, flood events, thermal anomalies. Parts of this uncertainty is artificially inflated because of the use of random values for initial coral cover at different reefs. As a result, model outputs (averages) are be accompanied by their coefficient of variation determined from replicate simulations.

Quantitative relationships can predict the quality of coral habitats (e.g. for fish) from the predicted community states, and, ultimately, fish productivity for reef valuation. A first approach uses field observations on reef structural complexity and coral community composition collected in Indonesia by Rogers et al. (2018). In this study, physical refuges of different sizes were counted on four replicate 10m×1m transects laid on 16 reef sites. Refuges were defined as any hole or crevice within the reef framework that offers physical protection to fish, including spaces within corals, between corals of different growth forms and underneath various overhanging structures. Two kinds of refuges were assessed:

Refuges within stands of branching corals; their density was estimated indirectly by measuring the area of branching colonies (length×width) assigned to either fine (1cm-2.5cm) or medium branching (2.5cm-5cm) space. Assuming an average branching coral consists of 2/3 branches and 1/3 branch space (estimated from image analysis), colony area was converted into refuge density by dividing the total branch space by the maximum branch space. The resulting metric is density of fine and medium branching refuges per site. For refuges outside stands of branching corals; their density was measured by sticking fish models of different size (5cm increments) inside holes and crevices of the reef framework made of dead carbonate and living non-branching corals (massive, encrusting, foliose, sub-massive and *Pocillopora*). The resulting metric is density of refuges per size class per site.

Because the two metrics relate to different substrata (branching and non-branching), separate relationships can be derived to estimate the density of refuges from benthic cover data.

For the 14 sites where branching colonies have been surveyed, we determined the relationship between the cumulative density of refuges within fine and medium branching corals and the percent area covered by these colonies along the 10m transects (Fig. 43A):

RBranching = 4.596 + 6.241 percent branching

For the 16 sites, the cumulative density of all refuge sizes measured outside branching corals was related to the percent area covered by non-branching corals (Fig. 43B). Because benthic composition for non-branching corals was not estimated on the 10m x 1m transects, we used nearby assessments performed online-intercept transects:

RNonBranching = 1.468 (percent non-branching) ^ 0.878

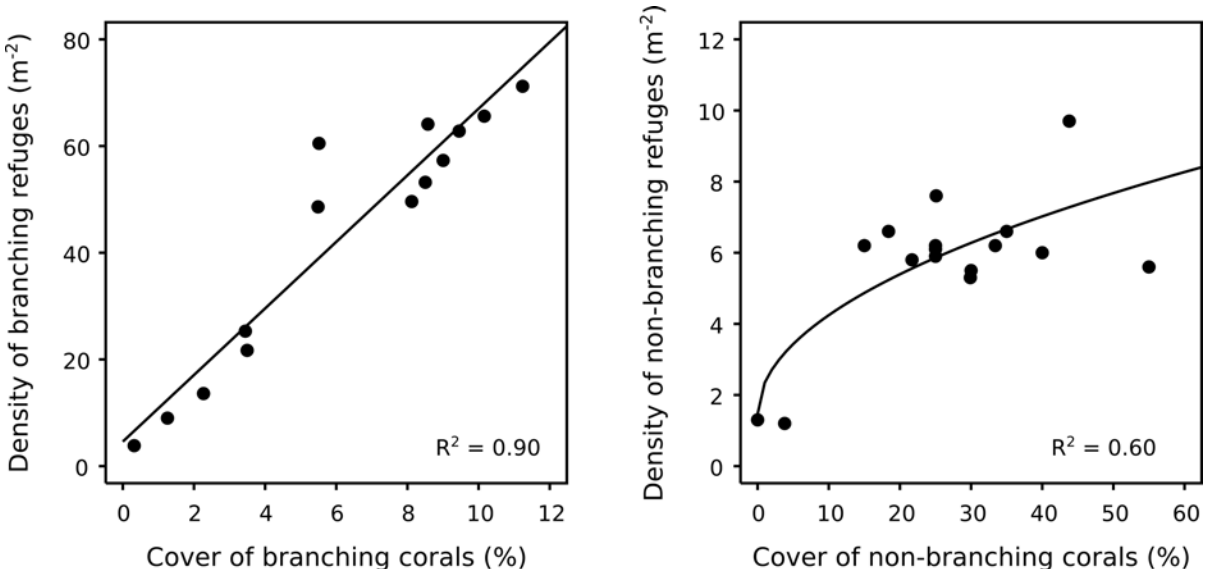

Figure 43: Empirical relationships between refuge density and the cover of branching and non-branching corals

With these two relationships we can obtain rough estimates of refuge density from the cover of branching Acropora and the cover of all other corals predicted by ReefMod. Once a value of structural complexity (refuge density) is assigned to a reef, we can further infer fish productivity and biomass following Rogers et al. (2018) model predictions (Fig. 44):

Fprod = 22.214 + 0.610 R – 0.009 R2
Pbiom = 23.873 + 1.614 R – 0.014 R2
with R = RBranching + RNonBranching

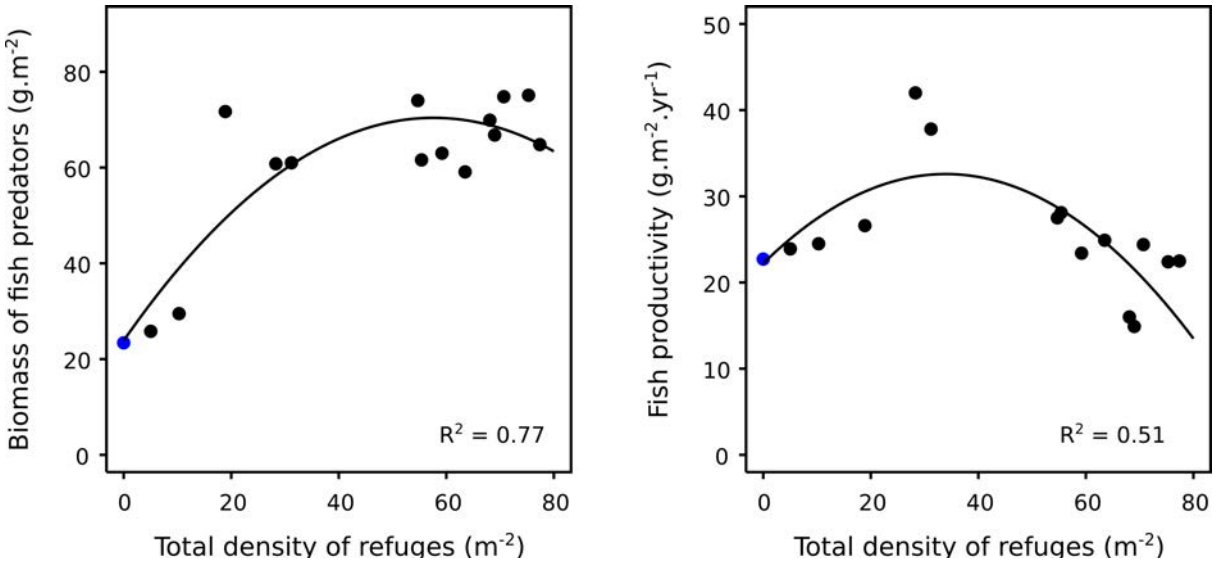

Figure 44: Estimates of fish productivity and predator biomass from a size-based ecosystem model (Rogers et al. 2014) for the refuge density estimated in Indonesia (modified from Rogers et al. 2018). Blue dot = ecosystem model's expectation with no refuge.

This approach has limitations. First, the functional impact of tabular corals is not captured because these corals were rarely encountered during Indonesian field surveys. Moreover, large overhangs and other crevices in excess of 50cm in length were not assessed as Rogers et al. (2018)'s model did not represent fish larger than this body size. Second, this approach gives a

disproportionate weight to branching corals as they largely drive the number of refuges (Fig.43). Finally, this assumes that branching corals disappear following mortality, while dead skeletons can still provide fish habitat before structural collapse due to mechanical erosion.

B2.2 Hindcast

B2.2.1 Parameterisation

To determine the initial conditions of reef state for the forecast simulations (i.e. coral cover as in 2018), 40 replicate simulations were run with spatially and temporally realistic regimes of water quality, crown-of-thorns starfish, bleaching and cyclones between 2008 and 2017 (10 years).

Initial benthic cover

For each replicate simulation, the initial coral cover for a given reef was randomly generated from a normal distribution centred on a predefined average (standard deviation: 10 percent). Average coral cover at the initial step was derived from data collected by the AIMS Long-term Monitoring Program in 2006-2007. This dataset provided reef-wide coral cover for more than 80 reefs across the entire Reef. The other reefs were initialised with the mean coral cover reported for each management sector and shelf position (inner-, mid- and outer-shelf reefs). Initial total coral cover for all reefs was distributed among the 6 functional groups following rough average community composition reported by AIMS Long-term Monitoring Program on the inner-, mid and outer-shelf reefs. The cover of rubble and ungrazable substratum (i.e. sand) are randomly generated from a normal distribution with mean 10 percent and standard deviation 10 percent.

Water quality regime

Water quality regime and impact on coral demographics during 2008–2017 was reproduced by selecting at every time step a spatial layer of coral reproduction success, recruit survival of Acropora corals and juvenile growth representative of the 2011–2016 regime of suspended sediments. The missing years were completed with the available layers assuming the period 2011–2016 is roughly representative of a cycling regime of rainfall, river flow and sediment transport across the Reef. Inter-annual variability was maintained by imposing the 2014–2016 seasonal layers to the simulated period 2008–2010, and the 2011 layers to the simulated year 2017.

Exposure to crown-of-thorns starfish outbreaks

Exposure to crown-of-thorns starfish outbreaks during 2008–2017 was reproduced by combining observational data with demographic simulations for reefs where no field observation was available. Manta tows from the Great Barrier Reef Marine Park Authority's Field Management Program (FMP) and AIMS Long-term Monitoring Program were used to inform crown-of-thorns starfish population densities on ~6 percent of all reefs (242 out of 3,806 reefs). This led to exposure layers with indicator values of -1 (no observation available), 0 (no outbreak detected), 1 (incipient outbreak) and 2 (active outbreak). At initialisation, reefs not surveyed and reefs with no detected outbreak were set with a null density of crown-of-thorns starfish. Reefs with incipient and active outbreaks were initialised with the median values of crown-of-thorns starfish densities reported by FMP manta tows (respectively 2075 and 7450 adult crown-of-thorns starfish per km^2, roughly equivalent to 0.3 and 1.1 adult crown-of-thorns starfish per tow, Moran and De'Ath 1992). For outbreaking populations, density-at-age (six-month classes) was generated from reference age distributions as determined by the demographic model underage-specific mortality and constant recruitment, assuming incipient and active outbreaks have been developing, from scratch, for three and five years respectively. Density-at-age was corrected for imperfect detectability using empirical predictions from MacNeil et al. (2016). At the following steps, crown-

of-thorns starfish populations on reefs that were not surveyed in a given year were estimated by the model based on standing populations and larval connectivity, while reefs surveyed that year were imposed the corresponding reference population (i.e. absent, incipient or active outbreaking described above) in such a way that preference was always given to field observations.

Exposure to thermal stress

Past degree heating weeks records for the 3806 reefs were derived from Hock et al. (2017) which combines satellite data from the Coral Reef Temperature Anomaly Database (CoRTAD version 5) for years prior to 2012 (Casey et al. 2015) and data from ReefTemp Next Generation (Garde et al. 2014). The reconstructed regime of thermal stress captures the most recent (2016-2017) bleaching events.

Exposure to cyclones

Spatially explicit hindcast of exposure to cyclone was generated from sea-state predictions of wave height (Puotinen et al. 2016). The potential for coral-damaging sea state (wave height >4m, Puotinen et al. 2016) was determined using a map of wind speed every hour within 4km pixels over the Reef for cyclones between 2008 and 2017. Any areas containing a combination of wind speed and duration capable of generating 4m waves, assuming sufficient fetch, were scored as positive for potential coral-damaging sea-state in the respective year. For each year, occurrence of damaging wave height was interpolated to the 3806 reefs, and where damaging waves were predicted to occur, coral mortality was estimated from the cyclone category (Saffir-Simpson scale) derived from the closest estimate of maximum mean along the cyclone track as provided by the Database of Past Tropical Cyclone Tracks of the Australian Bureau of Meteorology.

Outputs: coral condition in 2018 across the entire Reef and in the Cairns region

An overall view of present-day coral conditions across the entire Reef, as estimated from hindcast (2008–2017) simulations, is presented on Fig 45. This picture includes cover predictions for the six coral groups for 3806 reef polygons. The reef surface associated to each reef polygon was derived from the indicative reef outline (~0m-10m) provided by the Great Barrier Reef Marine Park Authority data on the Reef boundaries (Great Barrier Reef Marine Park Authority 2007).

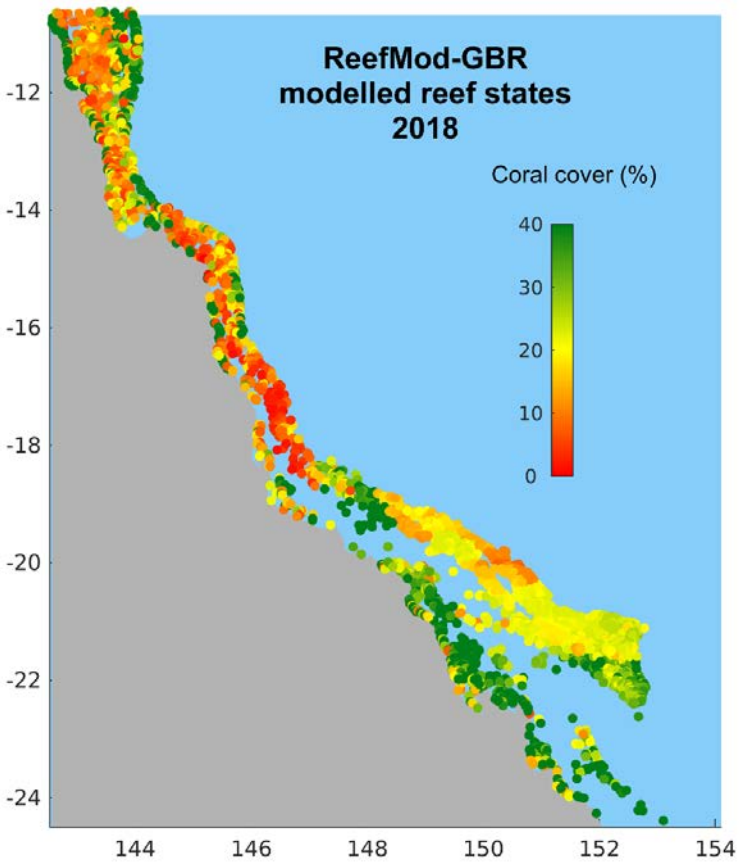

Figure 45: Result of hindcast simulations leading to the estimate of present-day (2018) coral condition (total coral cover) across 3806 reefs of the Great Barrier Reef.

A focus on the Cairns section is presented on Fig. 46 as this region benefits from recent high-resolution habitat mapping (C. Roelfsema, The University of Queensland). This mapping product is derived from satellite imagery and an object-based analysis for defining geomorphic zonation and bottom type (Roelfsema et al. 2018). At the start of the RRAP Concept Feasibility Study, the geomorphic maps were only available for the Cairns Management Area. Because they offer more precise estimates of reef surface areas, which is critical for estimating the deployment cost of many RRAP interventions, they were used for all the forward projections of coral condition (counterfactuals and interventions) presented hereafter. As a result, the benefits of RRAP interventions were only assessed on the Cairns section of the Reef. Since ReefMod is parameterised with coral demographic rates representative of a mid-depth (~5m–10m) reef environment, we only selected the reef slope habitat (3m-10m depth) as the modelled surface for every reef, leading to the selection of 156 reefs that exhibit a total reef slope area >0.17km^2.

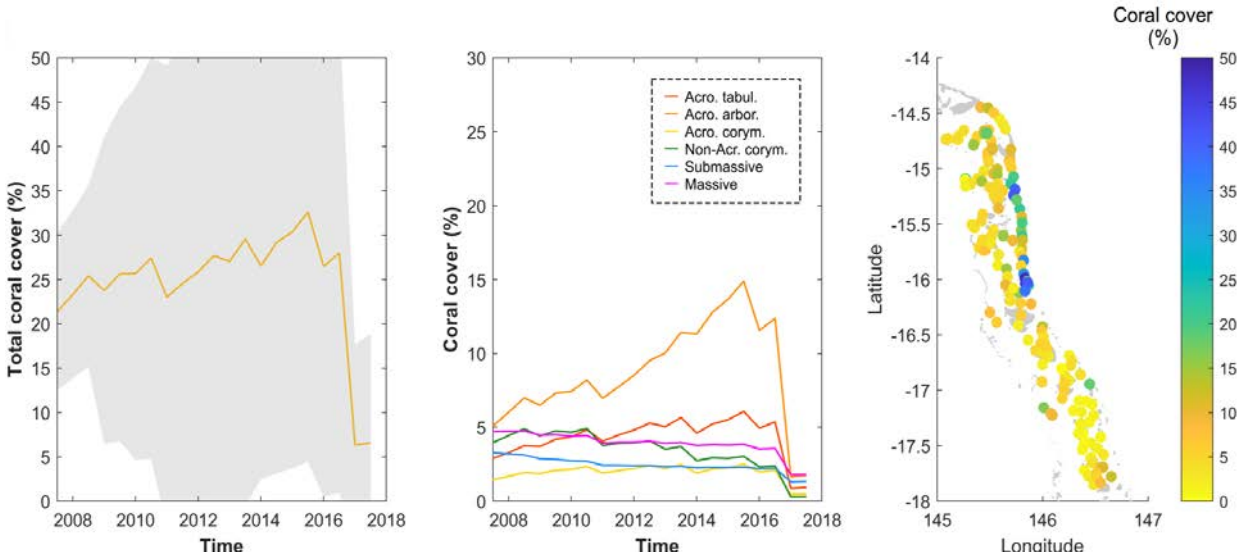

Figure 46: Hindcast reef trajectory in the Cairns region. (A) Averaged trajectory (orange) of the 156 reefs with a 90 percent confidence envelope (grey), calculated from the mean and variance (over 40 replicate runs) of the regionally averaged total coral cover weighted by reef areas. (B) Averaged trajectory of the six functional groups; (C) Map of the current (2018) state of the 156 reefs as predicted by the model.

Validation of these hindcast simulations is still in progress. To determine the extent to which ReefMod-GBR can predict coral cover in changing environments with confidence, model predictions will be compared against the coral trajectories monitored by AIMS Long-term Monitoring Program for the period 2008 to 2017. We anticipate some discrepancies between observed and predicted reef state because location-specific disturbances may not be captured by our model parameter values. Some habitats may unexpectedly escape cyclone/crown-of-thorns starfish/bleaching damages and some habitats may have been impacted by disturbances that went undetected (including coral disease). Also, crown-of-thorns starfish control was not included in these hindcasts. As the model develops further and local processes are captured and used to continuously update and calibrate model functions, we expect that the predictive capacity of ReefMod will improve over time. For the purpose of the RRAP Concept Feasibility Study, these estimates of coral condition across the Cairns section must be considered as tentative predictions under specific assumptions of past stress exposure.

B2.2.2 Forecast: counterfactual scenarios

Forward projections (2018-2070) of coral cover under climate change were performed for the Cairns Management Areas from the coral condition estimated for each group by the hindcast simulations. This region includes Cooktown-Lizard Island, Cairns and Innisfail Management Areas and is represented by 156 individual reefs as defined by the most recent mapping of reef habitats.

Forward projections of reef water quality were obtained by repeating the 2011–2016 regime of suspended sediments in the same chronological order, from 2018 to 2070. Exposure to crown-of-thorns starfish outbreaks was simulated using forecast predictions of the CoCoNet model under the two warming scenarios RCP 2.6 and RCP 8.5 and a business-as-usual control effort (8 control vessels). CoCoNet forecast simulations provided mean and standard deviation of crown-of-thorns starfish per manta tow across the Reef (2096 reefs), based on the selection of 50 model runs that all had <12 percent average coral cover in 2018, which is assumed to be representative

of reef states within the Cairns region as predicted by ReefMod. The time series were interpolated to the 156 reefs. At every time step on a given reef, a number of crown-of-thorns starfish per tow is generated from a normal distribution using the mean and SD predicted by CoCoNet for that particular reef and year, and converted into an equivalent density for the crown-of-thorns starfish population relative to the area of the reef (assuming 0.22 crown-of-thorns starfish per tow represent 1500 crown-of-thorns starfish per km^2, Moran and De'Ath 1992). Crown-of-thorns starfish population density was disaggregated per age class using the reference age distribution of an outbreaking population (see section Hindcast) and corrected for imperfect detectability using empirical predictions from MacNeil et al. (2016).

Forward projections of sea surface temperature and thermal stress followed the methodology developed by Wolff et al. (2015, 2018). First, future climatology was derived from the UK Hadley Centre Global Environmental Model HadGEM2-ES following two scenarios of greenhouse gas emission and concentration: the representative concentration pathways (RCP) 2.6 and 8.5, which, respectively, predict a global warming of 1°C and 2.2°C by the end of the 21st century. The coarse (1×1° resolution) Hadgem RCP sea surface temperature trajectories were adjusted to every reef based on the difference between past (1985–1993, omitting '91 and '92) Hadisst (1×1°) and CoRTAD (4km×4km) climatology. By using this approach, each CoRTAD pixel has an associated Hadgem trajectory without altering the warming trends. The 3806 reef centroids were intersected with CoRTAD pixels to produce reef-by-reef projections of sea surface temperature.

To predict thermal stress, a maximum monthly mean temperature was calculated for each reef based on the CoRTAD 1985–1993 (omitting '91 and '92) climatology. Future monthly anomalies >1°C above the maximum monthly mean from the climatology were accumulated within a three-month window to calculate degree heating months. Degree heating months were converted into degree heating weeks by multiplying by 4.3 (weeks per month).

If all individuals of a specific coral species were assumed to have the same thermal sensitivity, thermal stress would be estimated by using a reference threshold (maximum monthly mean +1°C) above which temperature anomalies accumulate (Wolff et al. 2015, 2018). Here, thermal stress is assumed to be dependent on coral's optimum temperature of individual corals, so that calculations must consider temperature anomalies above different thresholds (Topt +4°C). Reef-specific thermal stress values were then calculated for a range of Topt values varying from 15 to 40°C by increments of 0.1°C. Specifically for each reef climatology, future monthly anomalies >4°C above each Topt value were accumulated within a three-month window to calculate Topt-specific degree heating months were converted into degree heating weeks (by multiplying by 4.3) for the two RCPs (2.6 and 8.5). This way, a risk of mortality specific to each coral (relative to their Topt) can be calculated for a particular reef and year.

Forward projections of cyclone exposure were based on recent (1970–2011) cyclone tracks following the methodology developed by Wolff et al. (2016). Briefly, reef-scale probabilities of a cyclone occurrence were estimated from the annual rate and clustering statistics for each reef polygon. These statistics were used to generate 100 regional-scale cyclone disturbance regimes (simulations) for the period 2018–2070. When a cyclone event occurred within a reef polygon for a given simulation/year, a cyclone was randomly selected from a pool of 7000 synthetic tracks associated with that grid cell (see details in Wolff et al. 2016). Finally, whether a model reef was impacted by a particular cyclone occurring within its grid cell depended on the path of the cyclone

and the extent of its damaging winds. Each track was disaggregated into cyclone categories 1–5 on the Australian Bureau of Meteorology scale based on maximum sustained circular winds. A buffer was applied to each category track using wind speed extents defined by Keim et al. (2007) and a method described in detail in Edwards et al. (2011). The approach was adjusted to the Southern Hemisphere (opposite storm wind extent asymmetry to northern hemisphere) and the differences between the Australian Bureau of Meteorology and Saffir–Simpson hurricane classification system. Model reefs were intersected with buffered cyclone tracks to determine which cyclones affected each reef and the category of wind they experienced. Because there is no overlap between the 1970–2011 database of cyclone tracks and the 2011–2016 water quality regime, the projected forcing of suspended sediment and chlorophyll concentrations is unrelated to the projected storm events.

Actual adaptation rates are uncertain with a wide range of possible values of heritability and thermal tolerance. While the parameter space of thermal adaptation will be fully explored in the RRAP R&D Program, only two adaptation scenarios were considered here by using the credible lower and upper bounds of thermal tolerance and heritability:

- A **low adaptation potential** whereby corals have a somewhat narrow thermal tolerance ($\sigma = 1$, implying a 39 percent drop in coral fitness when temperature mismatches Topt by 1°C, see Fig. 41C) with a low efficiency of trait transmission (esd = 2).
- A **high adaptation potential** whereby corals have a broad thermal tolerance ($\sigma = 2$, implying a 13 percent drop in coral fitness for a 1°C mismatch, see Fig. 41C) with strong heritability (esd = 0.5).

For the two warming scenarios, 40 model simulations were run to estimate an average trajectory for each of the 156 reefs of the Cairns region.

Model runs show significant outcome improvements between the low and high adaptation potentials under RCP 2.6 (Fig. 47). The mean coral cover across the Cairns region exhibits an upward trajectory following the 2017 bleaching event, indicating persistence in the long term. Outcomes are significantly greater under the optimistic scenario of thermal adaptation, although forward projections of coral cover (~15 percent coral cover on average by 2070) remain well below the hindcast pre-2016-17 bleaching reef states (~25 percent coral cover on average). Thus, while it seems there is scope for thermal adaptation and long-term persistence under a scenario of aggressive reductions of greenhouse gas emissions, model projections indicate that reefs in the Cairns region might remain in a poor state for decades (i.e. below 10 percent on average).

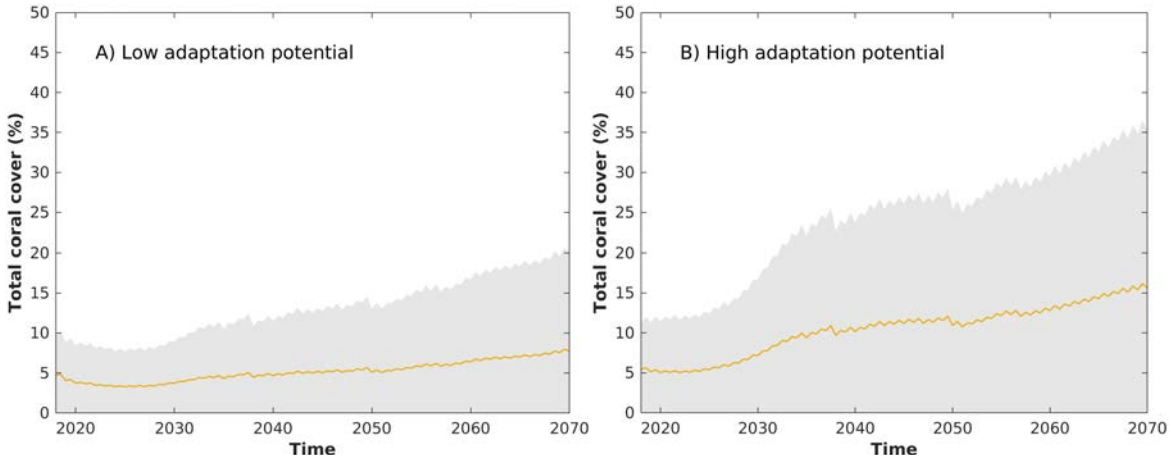

Figure 47: RCP 2.6 averaged trajectory (orange) of the 156 reefs in the Cairns region with a 90 percent confidence envelope (grey), calculated from the mean and variance (over 40 replicate runs) of the regional mean total coral cover weighted by reef areas.

Under a business-as-usual scenario of greenhouse gas emissions (RCP 8.5), the potential for thermal adaptation is impaired (Fig. 48). Under a low adaptation potential scenario, reefs in the Cairns region remain below 10 percent (~ five percent average across the region) throughout the modelled timeframe. Under a scenario of high adaptation potential, reefs seem to cope with the increasing regime of thermal stress until the middle of the century but fail to achieve persistence in the long term. The model suggests there is no scope for adaptation under business-as-usual greenhouse gas emissions.

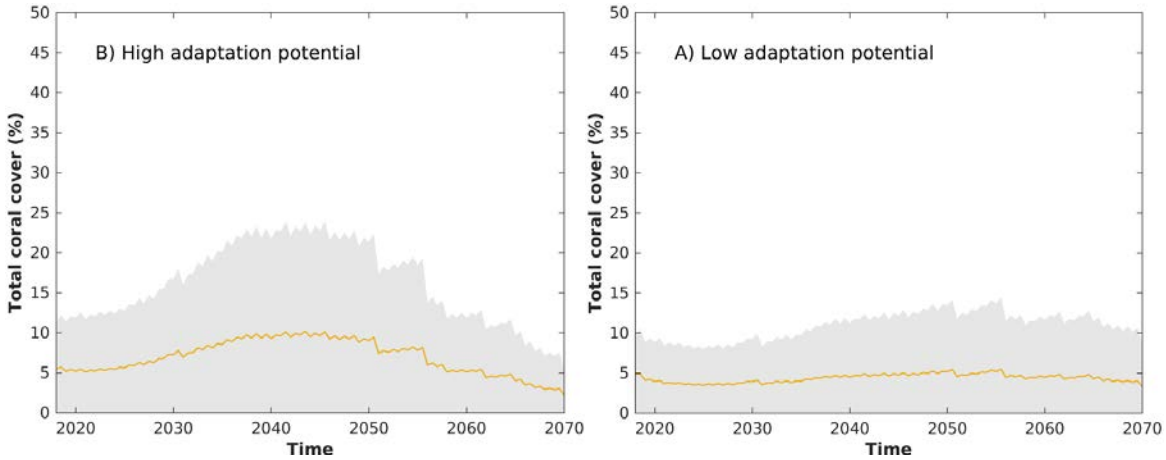

Figure 48: RCP 8.5 averaged trajectory (orange) of the 156 reefs in the Cairns region with a 90 percent confidence envelope (grey), calculated from the mean and variance (over 40 replicate runs) of the regional mean total coral cover weighted by reef areas.

B2.3 Forecast: RRAP interventions

B2.3.1 Outplanting of coral juveniles

As a spatially explicit, individual-based model, ReefMod is an efficient simulation tool to explore the performance and ecological benefits of outplanting coral individuals on the reef. Different strategies of coral deployment can be explored, whereby strategies refer to the use of different sizes (diameter) of corals (as nubbins, juveniles or adults), different densities of coral outplanting,

the number of restored reefs given their size and available amount of coral outplants, but also environmental characteristics that are likely to influence the success of the intervention at local (e.g., larval retention, water quality and exposure to acute stress) or regional scales (e.g. importance of the selected reef for supplying coral larvae to other reefs).

Coral outplanting was modelled as the addition of 2cm coral juveniles of plating and corymbose *Acropora* on a reef grid (400m^2). Corals were deployed once a year from 2025 onward at two densities: 0.5 and 1.0 coral juveniles per square metre. On a reef grid, the deployment is performed cell-by-cell following a stochastic process: the actual number of outplanted corals in a cell is determined at random following a Poisson distribution with the density of deployment as parameter. This number can be reduced following the current cell occupancy, with every cell being imposed a maximum 40 colonies per species. In addition, a cell cannot receive more than five coral juveniles. The genotype of deployed corals is created from the local pool of genes so that genetic diversity among the outplants reflects that of the native population. Thermal tolerance of outplants can be artificially increased by shifting their thermal optimum to warmer temperatures to simulate the outplanting of naturally or engineered warm-adapted corals. This is achieved by adding to the 20 quantitative trait loci of each outplanted coral 20 trait values selected at random, so that the breeding value elevates to the desired target (i.e. +1°C, +2°C). The model tracks the total number of corals effectively deployed across the 400 grid cells, which is scaled up to the representative habitat area of the reef, assuming for simplicity that the entire reef area is restored at the selected deployment density.

Simulations were performed for an increasing number of reefs in the Cairns region (i.e. 10, 20, 40, 60, 80 reefs out of 156) but only results for 10 and 20 restored reefs are presented since this deployment strategy required the production of a considerable amount of coral juveniles (between 20 and 80 million every year) yet the Cairns region represents only a small proportion of the Reef (~11 percent based on the area of 3806 reference reef polygons). The best donor reefs (i.e. reefs with the greatest number of larval connections with downstream reefs, referred as priority reefs) were selected assuming that local demographic benefits of coral outplanting may cascade through the network of larval connectivity. If a restored reef achieves a minimum 20 percent coral cover at any time step, restoration is stopped on that reef and the best donor reef down the list is selected for coral deployment. Outplanting is re-activated on priority reefs that eventually fall again below 20 percent coral cover. Ecological outcomes are assessed as the change in total coral cover for each reef at different points in time, relative to the counterfactual scenarios (two warming scenarios × two adaptation scenarios).

B2.3.2 Outplanting of coral juveniles with no increased thermal tolerance

Model runs show that the simulated densities of coral outplants (i.e., 0.5 and 1.0 coral juveniles per m^2) have relatively small effects on coral populations at the scale of a reef, and no detectable effects at the regional scale (Fig. 49-50). Local impact of coral deployment seems to be contingent on the current state of the restored reef with a very limited increase in coral cover obtained when depauperate reefs (i.e. below five percent cover) are targeted, probably a result of poor water quality (i.e. reefs with unfavourable conditions for juvenile growth). However, benefits of five to 10 percent can be achieved on some reefs if deployment occurs at relatively high densities (1.0 coral per m^2), although at this density the required amount of coral outplants (40-80 million a year) might be prohibitive. Local benefits seem to have no impact on downstream reefs, which suggests that larval supply is not significantly affected at the deployed densities.

10 restored reefs at density 0.5m^2 10 restored reefs at density 1.0m^2

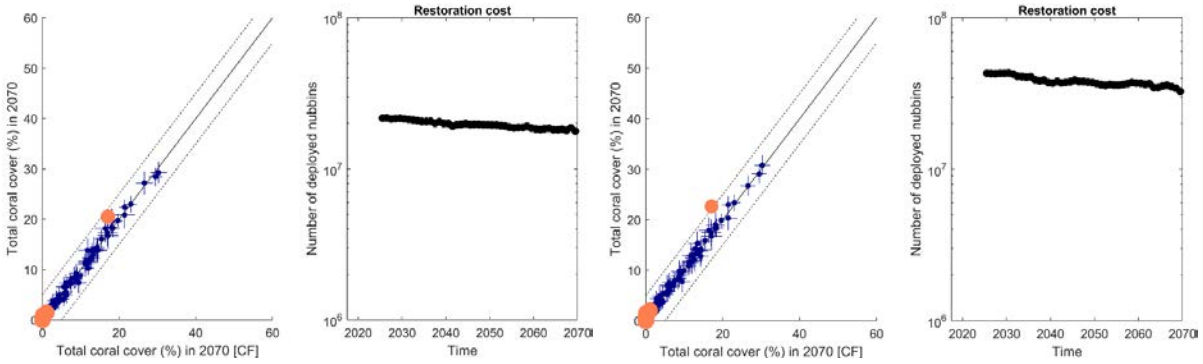

20 restored reefs at density 0.5m^2 20 restored reefs at density 1.0m^2

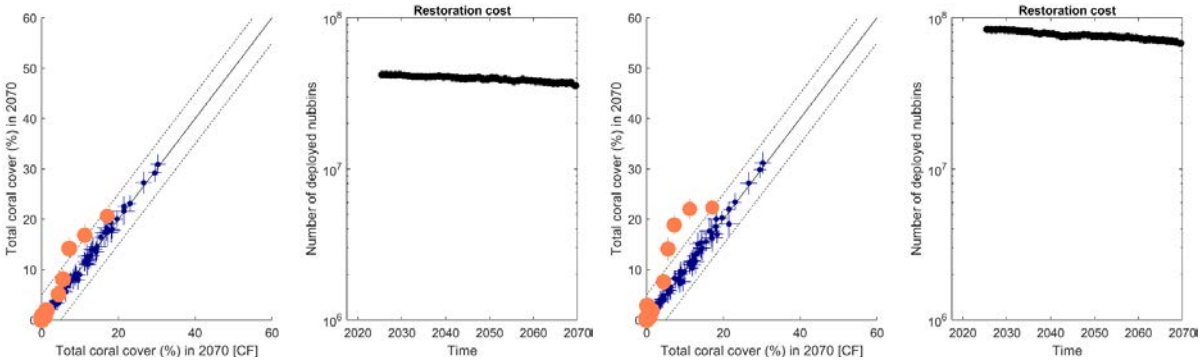

Fig.49: Long-term ecological benefits (left) and associated cost (right) of the deployment of coral juveniles across the Cairns region. Ecological benefits are measured in terms of total coral cover for the 156 reefs (dots) achieved by 2070 (y-axis) relative to the representative counterfactual scenario (x-axis). Reefs that were selected for coral deployment at least once over the simulated timeframe (i.e. priority reefs and eventual substitutes) are indicated using orange dots. Error bars indicate SD of reef coral cover over 40 replicate runs. Restoration cost is represented by the total number of coral juveniles deployed every year across the region (note the log scale) averaged over 40 runs. Simulations were performed under RCP 2.6 assuming a low potential of thermal adaptation, with deployed corals having the same thermal tolerance than native corals.

10 restored reefs at density 0.5m^2 10 restored reefs at density 1.0m^2

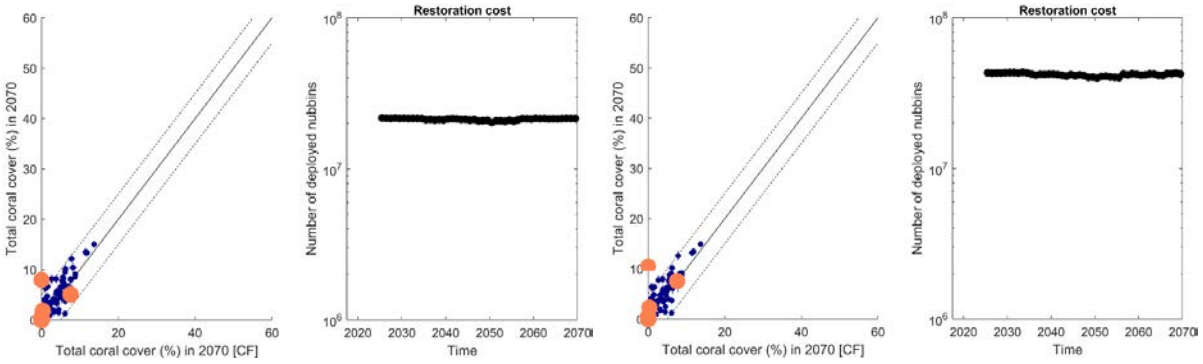

Fig.50: Long-term ecological benefits and associated cost of deploying coral juveniles with no increased thermal tolerance. Simulations were performed under RCP 8.5 assuming a low potential of thermal adaptation, with deployed corals having the same thermal tolerance than native corals.

More efficient strategies might be found by avoiding reefs with poor water quality. In addition, considering that larval supply on non-restored reef seems to be insensitive to coral deployment on reefs they are connected to, a more cost-effective approach could be to select reefs of smaller

size and/or by limiting coral deployment to a portion of a reef, assuming that the non-restored portion will benefit from larval retention. It is noteworthy that reef size is absolutely key to the estimated number of coral juveniles. Here, only a specific reef habitat was considered in the simulations: the leeward and windward reef slope environment from -3m to -10m depth. While the Cairns region benefits from the most accurate account of reef habitats, using reef areas informed by the Great Barrier Reef Marine Park Authority's indicative reef polygons would have produced far greater amounts of restoration costs (Fig. 51). This highlights the need of high-resolution mapping of colonisable hard-bottom reef habitats across the entire Reef for more accurate predictions of coral deployment costs.

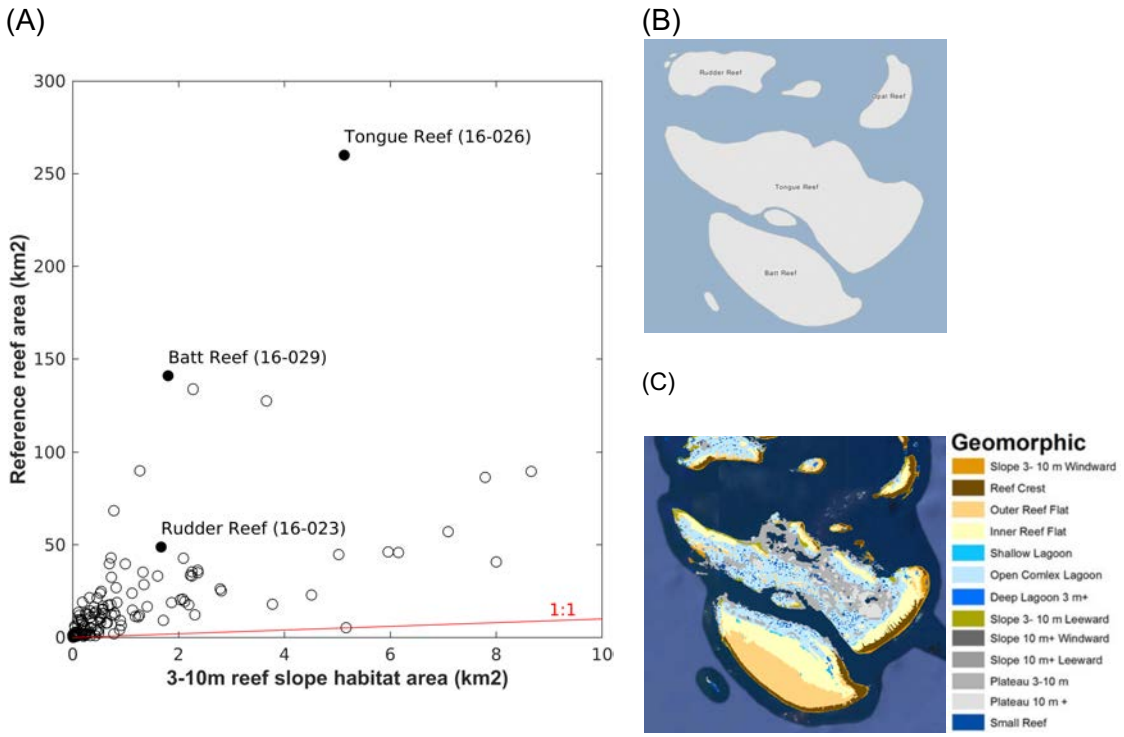

Fig. 51: (A) Relationship between the area of modelled habitat (3m-10m reef slope, only available for the Cairns region) and the reference area (Great Barrier Reef Marine Park Authority's indicative reef polygons, available for the entire GBR) for the 156 reefs. Using the reference reef areas (B) would incur restoration costs (i.e. number of coral juveniles deployed each year) on average 17 times greater than those currently estimated with the 3m-10m reef slope areas (C).

B2.3.3 Outplanting of coral juveniles with increasing thermal tolerance

Increasing the optimum temperature of coral outplants by 1°C (Fig. 52-53) or 2°C (Fig. 54-55) did not improve the outcomes of coral deployment. The simulated densities seem unable to change the composition of thermal traits across the region, despite a focus on the most connected reefs. While explanations could be the same as for the deployment of +0°C coral juveniles, another possible reason is that retention overrides external supply on those reefs. Moreover, selecting reefs that provide many dispersal routes could dilute the pool of larvae enriched with greater thermal tolerance; in this case, a more efficient strategy might be the selection of priority reefs that have fewer (yet strategic) connections to sink reefs.

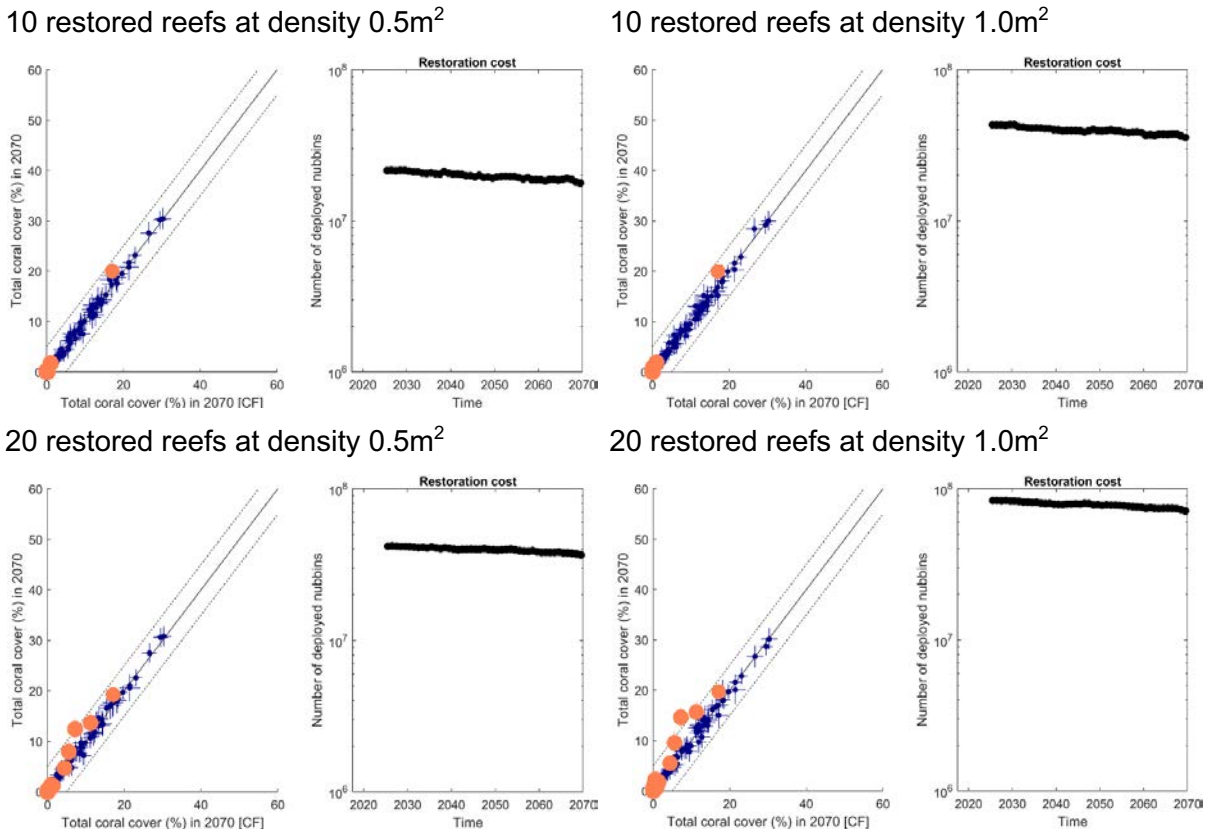

Fig.52: Long-term ecological benefits and associated cost of deploying coral juveniles with 1°C increased thermal tolerance. Simulations were performed under RCP 8.5 assuming a low potential of thermal adaptation.

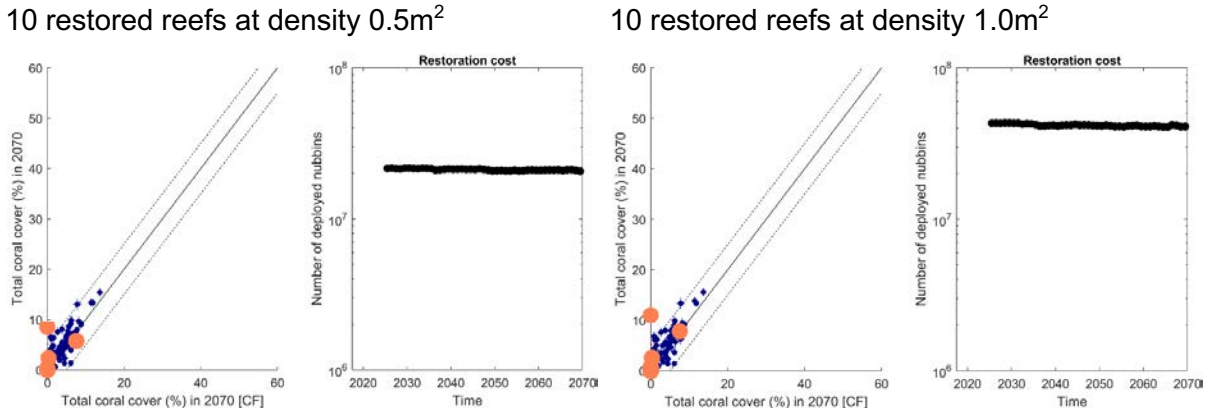

Fig. 53: Long-term ecological benefits and associated cost of deploying coral juveniles with 1°C increased thermal tolerance. Simulations were performed under RCP 8.5 assuming a low potential of thermal adaptation.

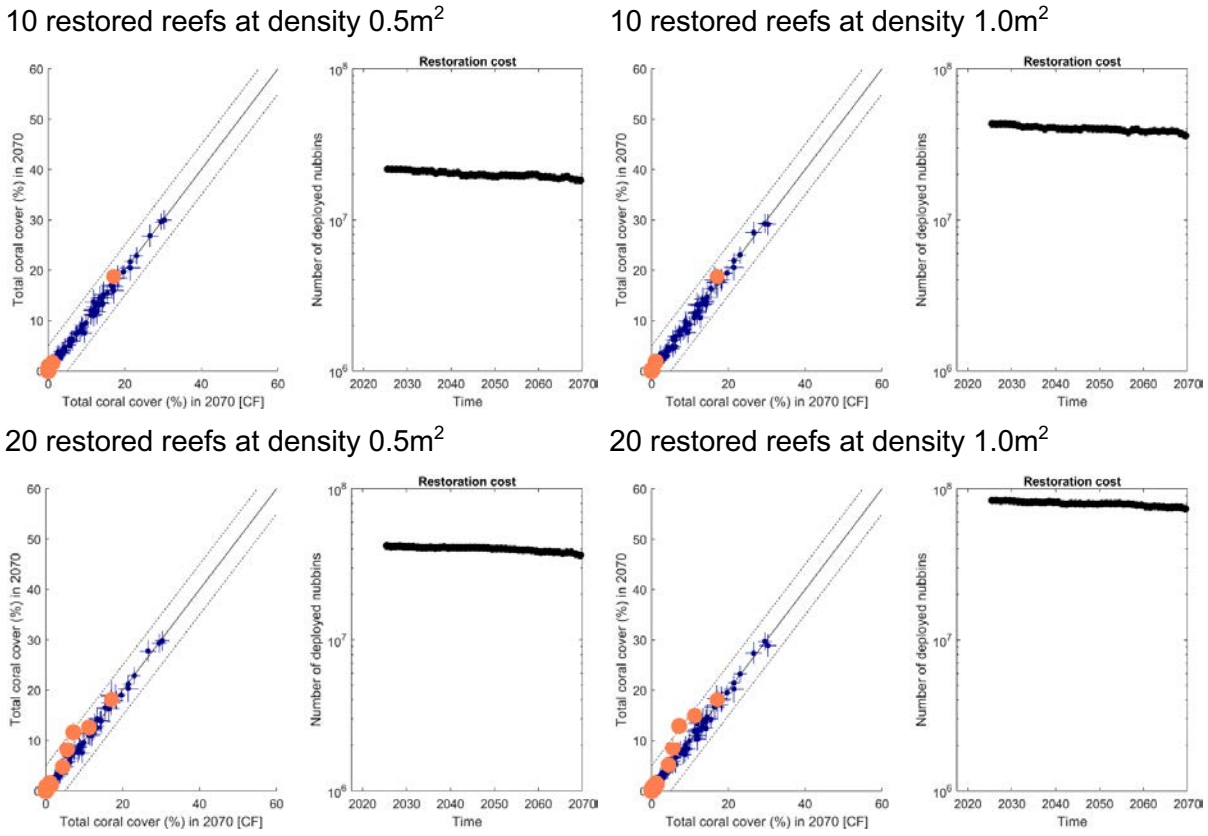

Fig.54: Long-term ecological benefits and associated cost of deploying coral juveniles with 2°C increased thermal tolerance. Simulations were performed under RCP 2.6 assuming a low potential of thermal adaptation.

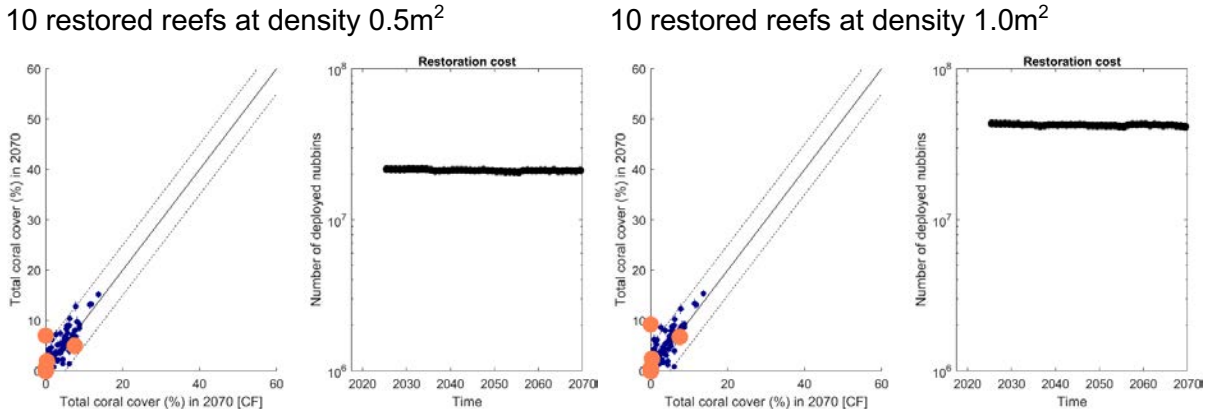

Fig.55: Long-term ecological benefits and associated cost of deploying coral juveniles with 2°C increased thermal tolerance. Simulations were performed under RCP 8.5 assuming a low potential of thermal adaptation.

B2.3.4 Solar radiation management

Solar radiation management was simulated as a direct cooling of sea surface temperature and reduction in the severity of heat stress predicted under the two warming scenarios (RCP 2.6 and RCP 8.5). Deployment of solar radiation management was assumed to begin in 2025 and was simulated every year onward for summer steps only. Three scenarios of cooling efficiency were tested by offsetting mean annual temperatures (sea surface temperature) by -0.3°C, -0.7°C and -1.3°C for a three-month equivalent period, resulting in an altered temperature regime potentially

affecting coral growth, fecundity, and, by extension, the dynamics of thermal adaptation. Reduction in cumulative heat stress was approximated by simply subtracting to the predicted degree heating weeks the cooling effect multiplied by 12, assuming solar radiation management operates over 12 consecutive weeks during the warmest summer months. This led to, respectively for the three cooling scenarios, a reduction of 3.6 degree heating weeks, 8.4 degree heating weeks and 15.6 degree heating weeks of the heat stress predicted for every increment of coral thermal optimum under each counterfactual scenario. Solar radiation management was assumed to be uniform across the Cairns region, so the same cooling effect was simulated for all reefs relative to their forecast climatology (2018-2070). Ecological benefits of solar radiation management were assessed through 40 replicate runs by comparing the regional mean coral cover with that obtained from the representative counterfactual.

Under RCP 2.6, solar radiation management has a significant impact by gradually increasing coral cover as the efficiency of cooling increases (Fig. 56). A region-wide benefit becomes apparent more than one decade after deployment and achieves a maximum five percent mean (i.e. regional average) coral cover by 2050 for the most efficient cooling effect (i.e. -1.3°C). The impact of artificial cooling is not uniform across the region with maximum local benefits around 10 percent coral cover (as estimated in 2070). Reefs exhibiting < five percent coral cover in 2070 are the least affected by solar radiation management. Ecological benefits are slightly greater under the optimistic scenario of coral adaptation.

Under RCP 8.5, solar radiation management has a greater impact with benefits for coral populations becoming apparent five years after deployment (Fig. 57). A maximum benefit of 10 percent mean coral cover is achieved under the greatest cooling efficiency, with maximum local benefits around 15 percent coral cover in 2070 including for low coral cover (i.e. <5 percent cover) reefs. The impact of solar radiation management is sensibly greater under the most optimistic scenario of thermal adaptation, with even higher benefits predicted to occur during the decade 2050–2060. These benefits, however, might not persist in the long term, as all cooling scenarios result in a declining reef trajectory by the end of the simulated timeframe. This suggests that, in the absence of drastic reductions of gas emissions, solar radiation management alone might be insufficient to ensure long-term reef persistence in the Cairns region.

(A) RCP 2.6, low adaptation potential

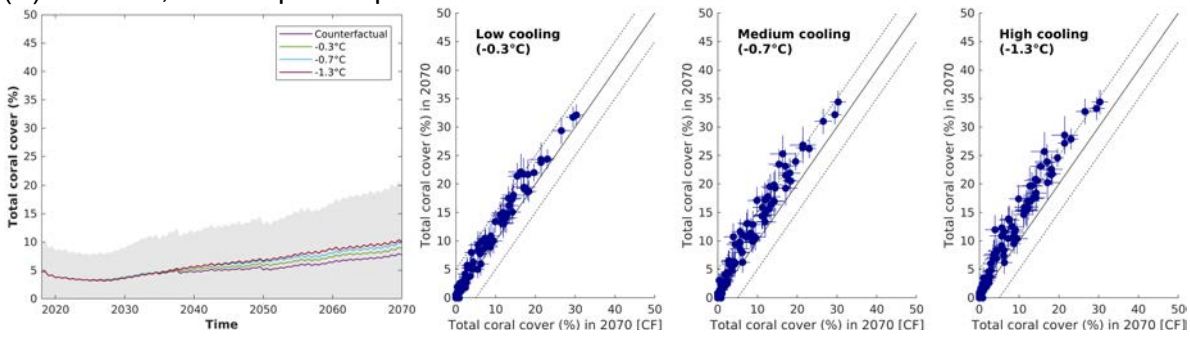

(B) RCP 2.6, high adaptation potential

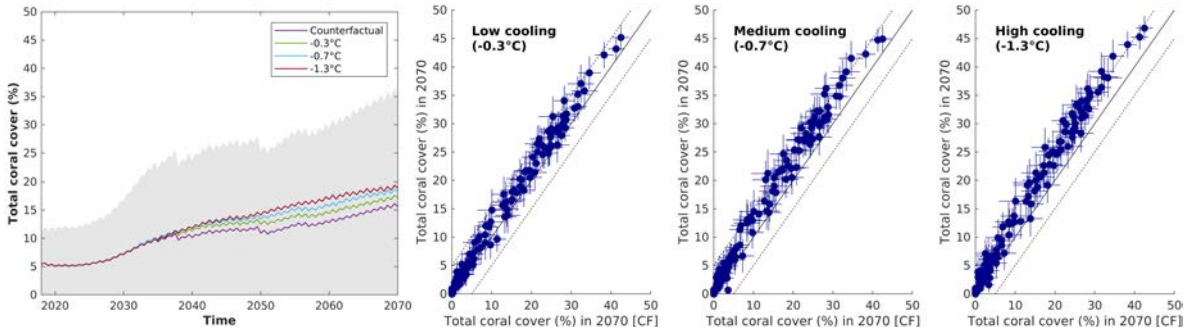

Fig. 56: Long-term ecological benefits of solar radiation management under low carbon emission (RCP 2.6) scenario.

(A) RCP 8.5, low adaptation potential

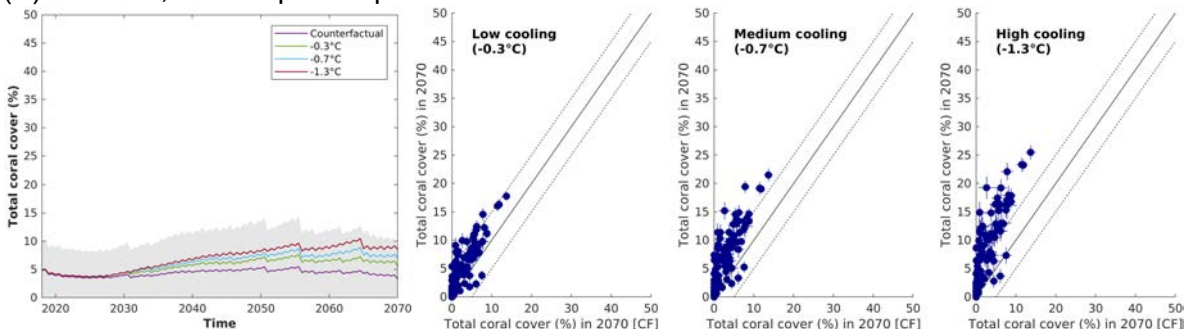

(B) RCP 8.5, high adaptation potential

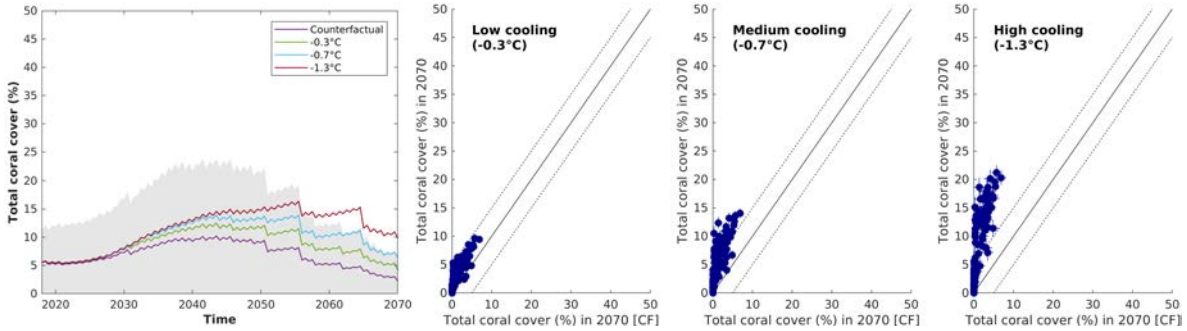

Fig.57: Long-term ecological benefits of solar radiation management brightening under low carbon emission (RCP 8.5) scenario

B2.3.5 Rubble stabilisation

Artificial stabilisation of loose rubble on the reef was modelled by setting rubble cover to 0 percent on reefs targeted for restoration, which results essentially in resetting coral juvenile survival to the default value (0.9 over six months). Simulations (2018–2070) were performed whereby 10 to 20 reefs are restored yearly from 2025 onward. Here again, the best donor reefs were used as priority reefs for intervention, provided that current rubble cover is above five percent in any given year. As for coral deployment, restoration moves to another reef down the priority list if rubble cover is below this threshold. Restoration cost is calculated every year as the total area of stabilised substratum across the Cairns region.

Under RCP 2.6 and low adaptation potential, rubble stabilisation has no detectable effect on the regional coral cover (Fig. 58). Being generated from coral loss after disturbance, rubble cover remains globally low (max. ~10 percent) due to the low levels of coral cover (max. ~10 percent) maintained on all reefs over the course of simulation (see Fig. 47A). Hence, the stabilisation of

small rubble beds (i.e. five-10 percent rubble cover) has a limited impact on the survival of juveniles which is close to the optimum value. Once a reef is restored and rubble cover set to 0 percent, it takes a long time before rubble exceeds five percent again because disturbances can only generate a small amount of rubble at a time, and most of it is rapidly stabilised by natural processes of cementation. As a result, reefs selected for intervention largely extend the priority list with many substitute reefs being visited at multiple occasions, so that restoring 10 or 20 reefs produces similar ecological outcomes and restoration costs.

Inversely, the impact of artificial rubble stabilisation appears significant under RCP 2.6 and high adaptation potential (Fig. 58B). This is essentially because corals achieve greater coverage (see Fig.47B) and so does rubble generated by acute disturbances. A slightly greater production of rubble (max. ~15 percent) is enough to affect coral demographics in such a way that the benefits of forced rubble stabilisation become substantial. While this highlights that loose rubble has a greater impact where corals are abundant, it merely reveals the magnitude of the negative feedback that impede coral recovery. One important implication is that healthy reefs today are likely to benefit the most from rubble stabilisation post-disturbance. It is certainly more cost-efficient to focus intervention on reefs where rubble is abundant rather than dispersing the restoration effort. Moreover, it can be anticipated that much greater regional benefits might be achieved with a strategy that optimises the sequence by which reefs are selected for rubble stabilisation. In particular, the threshold value of rubble cover used to trigger intervention is likely to have a disproportionate effect on the benefits measured at the scale of the region. Importantly, the impacts of rubble stabilisation can be overlooked in cost-benefit analyses based on pessimistic reef state projections, i.e. the ‘rubble problem’ is contingent to the amount of corals available prior to disturbance.

(A) RCP 2.6, low adaptation potential

10 restored reefs

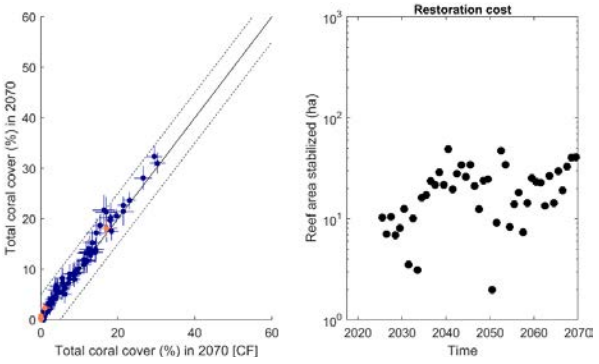

20 restored reefs

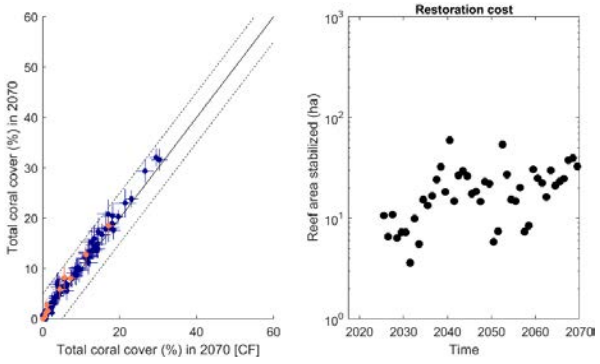

(B) RCP 2.6, high adaptation potential

10 restored reefs

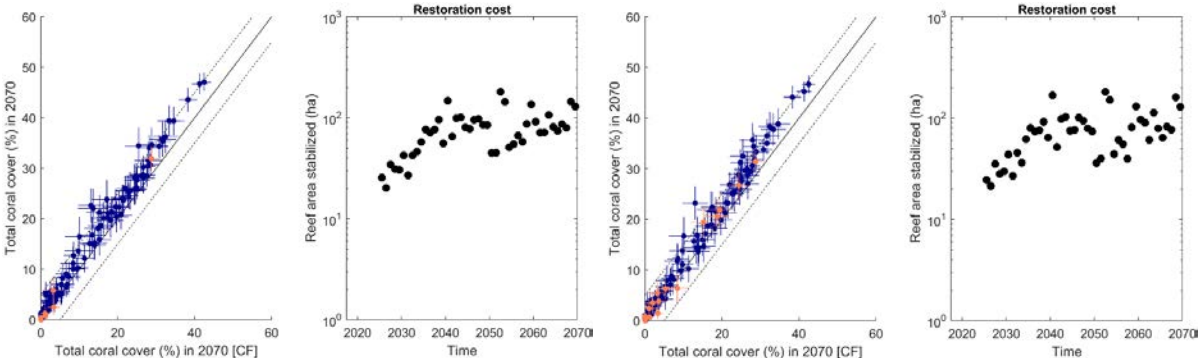

20 restored reefs

Fig.58: Long-term ecological benefits of rubble stabilisation under low carbon emissions (RCP 2.6). Orange dots indicate priority reefs. Error bars indicate SD of reef coral cover over 40 replicate runs.

Under RCP 8.5, rubble stabilisation has no noticeable effect on coral cover for any scenario of adaptation and deployment strategy (Fig.59). Similar to the RCP 2.6 scenario of low adaptation potential, reefs maintain levels of coral cover that are too low to create amounts of rubble after disturbance that can significantly impede juvenile survival.

(A) RCP 8.5, low adaptation potential

10 restored reefs

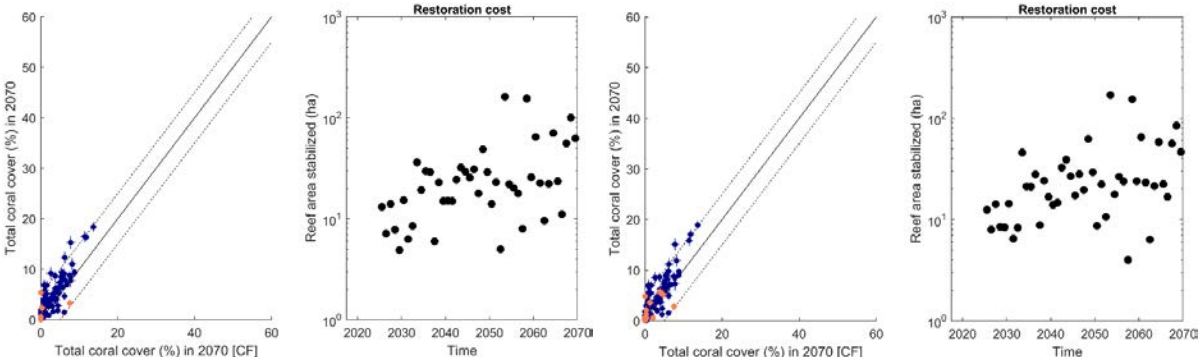

20 restored reefs

(B) RCP 8.5, high adaptation potential

10 restored reefs

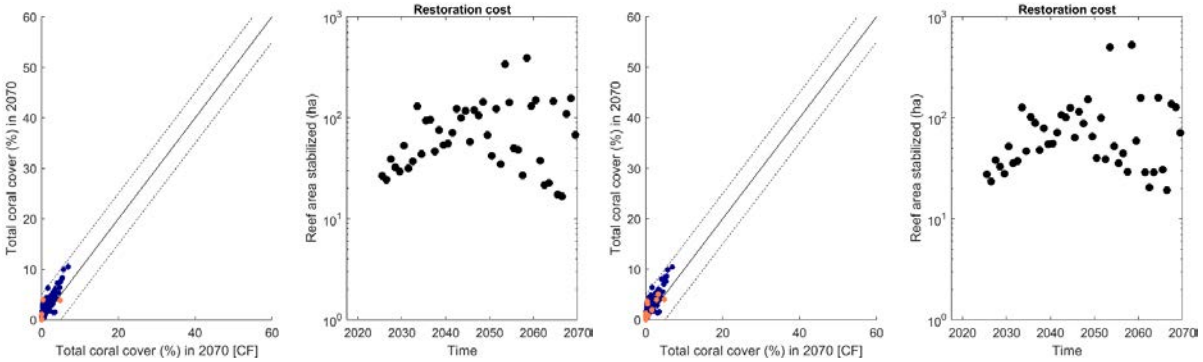

20 restored reefs

Fig.59: Long-term ecological benefits of rubble stabilisation under high carbon emissions (RCP 8.5).

Appendix B2 References

Anthony, K., M. O. Hoogenboom, J. A. Maynard, A. G. Grottoli, and R. Middlebrook. 2009. Energetics approach to predicting mortality risk from environmental stress: a case study of coral bleaching. Functional ecology 23:539–550.

Baird, A., and P. Marshall. 2002. Mortality, growth and reproduction in scleractinian corals following bleaching on the Great Barrier Reef. Marine Ecology Progress Series 237:133–141.

Baird, M. E., M. P. Adams, J. Andrewartha, N. Cherukuru, M. Gustafsson, S. Hadley, M. Herzfeld, E. Jones, N. Margvelashvili, M. Mongin, and others. 2017. CSIRO environmental modelling suite: scientific description of the optical, carbon chemistry and biogeochemical models (BGC1p0).

Baria, M. V. B., R. D. Villanueva, and J. R. Guest. 2012. Spawning of Three-Year-Old Acropora Millepora Corals Reared from Larvae in Northwestern Philippines. Bulletin of Marine Science 88:61–62.

Berkelmans, R. 2002. Time-integrated thermal bleaching thresholds of reefs and their variation on the Great Barrier Reef. Marine ecology progress series 229:73–82.

Biggs, B. C. 2013. Harnessing natural recovery processes to improve restoration outcomes: an experimental assessment of sponge-mediated coral reef restoration. PloS one 8:e64945.

Bozec, Y.-M., L. Yakob, S. Bejarano and P. J. Mumby. 2013. Reciprocal facilitation and non-linearity maintain habitat engineering on coral reefs. Oikos 122: 428-440.

Bozec, Y.-M., S. O'Farrell, J. H. Bruggemann, B. E. Luckhurst, and P. J. Mumby. 2016. Tradeoffs between fisheries harvest and the resilience of coral reefs. Proceedings of the National Academy of Sciences of the United States of America 113:4536–4541.

Bozec, Y.-M., L. Alvarez-Filip, and P. J. Mumby. 2015. The dynamics of architectural complexity on coral reefs under climate change. Global Change Biology 21:223–235.

Bozec, Y.-M., C. Doropoulos, G. Roff, and P. J. Mumby. 2019. Transient Grazing and the Dynamics of an Unanticipated Coral–Algal Phase Shift. Ecosystems 22:296-311..

Casey, K., E. Selig, D. Zhang, K. Saha, A. Krishnan, and E. McMichael. 2015. The Coral Reef Temperature Anomaly Database (CoRTAD) Version 5—Global, 4 km sea surface temperature and related thermal stress metrics for 1982–2012. NOAA National Centers for Environmental Information. Dataset. doi 10:V5CZ3545.

Chen, Y., S. Minchin, S. Seaton, K. Joehnk, B. Robson, Q. Bai, F. Chan, D. Marinova, and R. Anderssen. 2011. eReefs–a new perspective on the Great Barrier Reef. Pages 12–16 19th International Congress on Modelling and Simulation, Perth, Australia.

Condie, S. A., M. Hepburn, and J. Mansbridge. 2012. Modelling and visualisation of connectivity on the Great Barrier Reef. Pages 9–13 Proceedings of the 12th International Coral Reef Symposium.

Connell, J. H. 1997. Disturbance and recovery of coral assemblages. Coral reefs 16:S101–S113.

Connolly, S. R., and A. H. Baird. 2010. Estimating dispersal potential for marine larvae: dynamic models applied to scleractinian corals. Ecology 91:3572–3583.

Dollar, S., and G. Tribble. 1993. Recurrent storm disturbance and recovery: a long-term study of coral communities in Hawaii. Coral Reefs 12:223–233.

Doropoulos, C., G. Roff, Y.-M. Bozec, M. Zupan, J. Werminghausen, and P. J. Mumby. 2016. Characterizing the ecological trade-offs throughout the early ontogeny of coral recruitment. Ecological Monographs 86:20–44.

Doropoulos, C., S. Ward, G. Roff, M. González-Rivero, and P. J. Mumby. 2015. Linking demographic processes of juvenile corals to benthic recovery trajectories in two common reef habitats. PLoS One 10:e0128535.

Edmunds, P. J. 2005. The effect of sub-lethal increases in temperature on the growth and population trajectories of three scleractinian corals on the southern Great Barrier Reef. Oecologia 146:350–364.

Edwards, H. J., I. A. Elliott, C. M. Eakin, A. Irikawa, J. S. Madin, M. McField, J. A. Morgan, R. van Woesik, and P. J. Mumby. 2011. How much time can herbivore protection buy for coral reefs under realistic regimes of hurricanes and coral bleaching? Global Change Biology 17:2033–2048.

Emslie, M., A. Cheal, H. Sweatman, and S. Delean. 2008. Recovery from disturbance of coral and reef fish communities on the Great Barrier Reef, Australia. Marine Ecology Progress Series 371:177–190.

Fabricius, K., K. Okaji, and G. De'Ath. 2010. Three lines of evidence to link outbreaks of the crown-of-thorns seastarcrown-of-thorns starfish Acanthaster planci to the release of larval food limitation. Coral Reefs 29:593–605.

Fox, H. E., J. S. Pet, R. Dahuri, and R. L. Caldwell. 2003. Recovery in rubble fields: long-term impacts of blast fishing. Marine Pollution Bulletin 46:1024–1031.

Garde, L., C. Spillman, S. Heron, and R. Beeden. 2014. Reef Temp Next Generation: A new operational system for monitoring reef thermal stress. Journal of Operational Oceanography 7:21–33.

Great Barrier Reef Marine Park Authority. 2007. Great Barrier Reef (GBRReef) Features (Reef boundaries, QLD Mainland, Islands, Cays, Rocks and Dry Reefs) (GBRMPA). eAtlas.

Hall, V., and T. Hughes. 1996. Reproductive strategies of modular organisms: comparative studies of reef-building corals. Ecology 77:950–963.

Herzfeld, M., J. Andrewartha, M. Baird, R. Brinkman, M. Furnas, P. Gillibrand, M. Hemer, K. Joehnk, E. Jones, D. McKinnon, and others. 2016. eReefs Marine Modelling: Final Report, Jan. 2016, CSIRO, Hobart, 497 pp.

Hock, K., N. H. Wolff, S. A. Condie, K. Anthony, and P. J. Mumby. 2014. Connectivity networks reveal the risks of crown-of-thorns starfish outbreaks on the Great Barrier Reef. Journal of applied ecology 51:1188–1196.

Hock, K., N. H. Wolff, J. C. Ortiz, S. A. Condie, K. R. Anthony, P. G. Blackwell, and P. J. Mumby. 2017. Connectivity and systemic resilience of the Great Barrier Reef. PLoS biology 15:e2003355.

Hughes, T. P., J. T. Kerry, M. Álvarez-Noriega, J. G. Álvarez-Romero, K. D. Anderson, A. H. Baird, R. C. Babcock, M. Beger, D. R. Bellwood, R. Berkelmans, and others. 2017. Global warming and recurrent mass bleaching of corals. Nature 543:373.

Hughes, T. P., J. T. Kerry, A. H. Baird, S. R. Connolly, A. Dietzel, C. M. Eakin, S. F. Heron, A. S. Hoey, M. O. Hoogenboom, G. Liu, and others. 2018. Global warming transforms coral reef assemblages. Nature 556:492.

Humanes, A., A. Fink, B. L. Willis, K. E. Fabricius, D. de Beer, and A. P. Negri. 2017a. Effects of suspended sediments and nutrient enrichment on juvenile corals. Marine pollution bulletin 125:166–175.

Humanes, A., G. F. Ricardo, B. L. Willis, K. E. Fabricius, and A. P. Negri. 2017b. Cumulative effects of suspended sediments, organic nutrients and temperature stress on early life history stages of the coral Acropora tenuis. Scientific reports 7:44101.

Jones, R., G. Ricardo, and A. Negri. 2015. Effects of sediments on the reproductive cycle of corals. Marine Pollution Bulletin 100:13–33.

Keesing, J., and J. Lucas. 1992. Field measurement of feeding and movement rates of the crown-of-thorns starfish Acanthaster planci (L.). Journal of experimental marine biology and ecology 156:89–104.

Keim, B. D., R. A. Muller, and G. W. Stone. 2007. Spatiotemporal patterns and return periods of tropical storm and hurricane strikes from Texas to Maine. Journal of climate 20:3498–3509.

Kettle, B., and J. Lucas. 1987. Biometric relationships between organ indices, fecundity, oxygen consumption and body size in Acanthaster planci (L.)(Echinodermata; Asteroidea). Bulletin of Marine Science 41:541–551.

MacNeil, M. A., C. Mellin, M. S. Pratchett, J. Hoey, K. R. Anthony, A. J. Cheal, I. Miller, H. Sweatman, Z. L. Cowan, S. Taylor, and others. 2016. Joint estimation of crown of thorns (Acanthaster planci) densities on the Great Barrier Reef. PeerJ 4:e2310.

Marshall, A. T., and P. Clode. 2004. Calcification rate and the effect of temperature in a zooxanthellate and an azooxanthellate scleractinian reef coral. Coral reefs 23:218–224.

Matz, M. V., E. A. Treml, G. V. Aglyamova, and L. K. Bay. 2018. Potential and limits for rapid genetic adaptation to warming in a Great Barrier Reef coral. PLoS genetics 14:e1007220.

Moran, P., and G. De'Ath. 1992. Estimates of the abundance of the crown-of-throns starfish Acanthaster planci in outbreaking and non-outbreaking populations on reefs within the Great Barrier Reef. Marine Biology 113:509–515.

Mumby P. J. 1999 Bleaching and hurricane disturbances to populations of coral recruits in Belize. Marine Ecology Progress Series 190, 27–35.

Mumby, P. J. 2006. The impact of exploiting grazers (Scaridae) on the dynamics of Caribbean coral reefs. Ecological Applications 16:747-769.

Mumby, P. J., A. Hastings, and H. J. Edwards. 2007. Thresholds and the resilience of Caribbean coral reefs. Nature 450:98–101.

Mumby, P. J., N. H. Wolff, Y.-M. Bozec, I. Chollett, and P. Halloran. 2014. Operationalizing the resilience of coral reefs in an era of climate change. Conservation Letters 7:176–187.

Ortiz, J. C., Y.-M. Bozec, N. H. Wolff, C. Doropoulos, and P. J. Mumby. 2014. Global disparity in the ecological benefits of reducing carbon emissions for coral reefs. Nature Climate Change 4:1090.

Pratchett, M. S., C. F. Caballes, J. A. Rivera-Posada, and H. P. Sweatman. 2014. Limits to understanding and managing outbreaks of crown-of-thorns starfish (Acanthaster spp.). Oceanography and Marine Biology: An Annual Review 52:133–200.

Puotinen, M., J. A. Maynard, R. Beeden, B. Radford, and G. J. Williams. 2016. A robust operational model for predicting where tropical cyclone waves damage coral reefs. Scientific reports 6:26009.

Rasser, M., and B. Riegl. 2002. Holocene coral reef rubble and its binding agents. Coral Reefs 21:57–72.

Richmond, R. H. 1997. Reproduction and recruitment in corals: critical links in the persistence of reefs. Life and death of coral reefs. Chapman & Hall, New York:175–197.

Robson, B. J., M. Baird, and K. Wild-Allen. 2013. A physiological model for the marine cyanobacteria, Trichodesmium. Pages 978–0 MODSIM2013, 20th International Congress on Modelling and Simulation. Modelling and Simulation Society of Australia and New Zealand, ISBN.

Roelfsema, C., Kovacs, E., Roos, P., Terzano, D., Lyons, M., & Phinn, S. (2018). Use of a semi-automated object-based analysis to map benthic composition, Heron Reef, Southern Great Barrier Reef. Remote Sensing Letters, 9(4), 324-333.

Rogers, A., J. L. Blanchard, S. P. Newman, C. S. Dryden, and P. J. Mumby. 2018. High refuge availability on coral reefs increases the vulnerability of reef-associated predators to overexploitation. Ecology 99:450–463.

Sano, M., M. Shimizu, and Y. Nose. 1987. Long-term effects of destruction of hermatypic corals by Acanthaster planci infestation on reef fish communities at Iriomote Island, Japan. Marine Ecology Progress Series:191–199.

Trapon, M. L., M. S. Pratchett, and A. S. Hoey. 2013. Spatial variation in abundance, size and orientation of juvenile corals related to the biomass of parrotfishes on the Great Barrier Reef, Australia. PloS one 8:e57788.

Vermeij, M. J., and S. A. Sandin. 2008. Density-dependent settlement and mortality structure the earliest life phases of a coral population. Ecology 89:1994–2004.

Viehman, T. S., J. L. Hench, S. P. Griffin, A. Malhotra, K. Egan, and P. N. Halpin. 2018. Understanding differential patterns in coral reef recovery: chronic hydrodynamic disturbance as a limiting mechanism for coral colonization. Marine Ecology Progress Series 605:135–150.

Wallace, C. 1999. Staghorn corals of the world: a revision of the genus Acropora. CSIRO publishing.

Wolff, N. H., S. D. Donner, L. Cao, R. Iglesias-Prieto, P. F. Sale, and P. J. Mumby. 2015. Global inequities between polluters and the polluted: climate change impacts on coral reefs. Global Change Biology 21:3982–3994.

Wolff, N. H., P. J. Mumby, M. Devlin, and K. Anthony. 2018. Vulnerability of the Great Barrier Reef to climate change and local pressures. Global change biology.

Wolff, N. H., A. Wong, R. Vitolo, K. Stolberg, K. R. Anthony, and P. J. Mumby. 2016. Temporal clustering of tropical cyclones on the Great Barrier Reef and its ecological importance. Coral Reefs 35:613–623.

Reef Restoration and Adaptation Program

GBRrestoration.org

Ken Anthony
Australian Institute of Marine Science
k.anthony@aims.gov.au

Reef Restoration and Adaptation Program, a partnership:

Australian Government | Australian Institute of Marine Science | Australian Government Great Barrier Reef Marine Park Authority | Great Barrier Reef Foundation | CSIRO | QUT | James Cook University Australia | The University of Queensland Australia